# Annotating DHA Metabolites Interfering with the Quantification of Emerging Perfluoroalkyl Ether Carboxylic Acids

Yuyan Ji[1], Yitao Pan[1*], Jean-Marie Galano[2], Ángel Sánchez-Illana[3], Xinchen Miao[1], Fengfeng Dong[1], Camille Oger[2], Thierry Durand[2], and Jiayin Dai[1]

[1]State Environmental Protection Key Laboratory of Environmental Health Impact Assessment of Emerging Contaminants, School of Environmental Science and Engineering, Shanghai Jiao Tong University, Shanghai 200240, China.

[2]Institut des Biomolécules Max Mousseron (IBMM), Pôle Chimie Balard Recherche, UMR 5247, Université de Montpellier, CNRS, ENSCM, Montpellier, 340093, France.

[3]Department of Analytical Chemistry, University of Valencia, Burjassot, 46100, Spain.

***Correspondence author:** Yitao Pan, State Environmental Protection Key Laboratory of Environmental Health Impact Assessment of Emerging Contaminants, School of Environmental Science and Engineering, Shanghai Jiao Tong University, 800 Dongchuan Road, Shanghai 200240, China. E-mail: panyitao@sjtu.edu.cn

**Competing financial interests:** The authors declare no conflicts of interest.

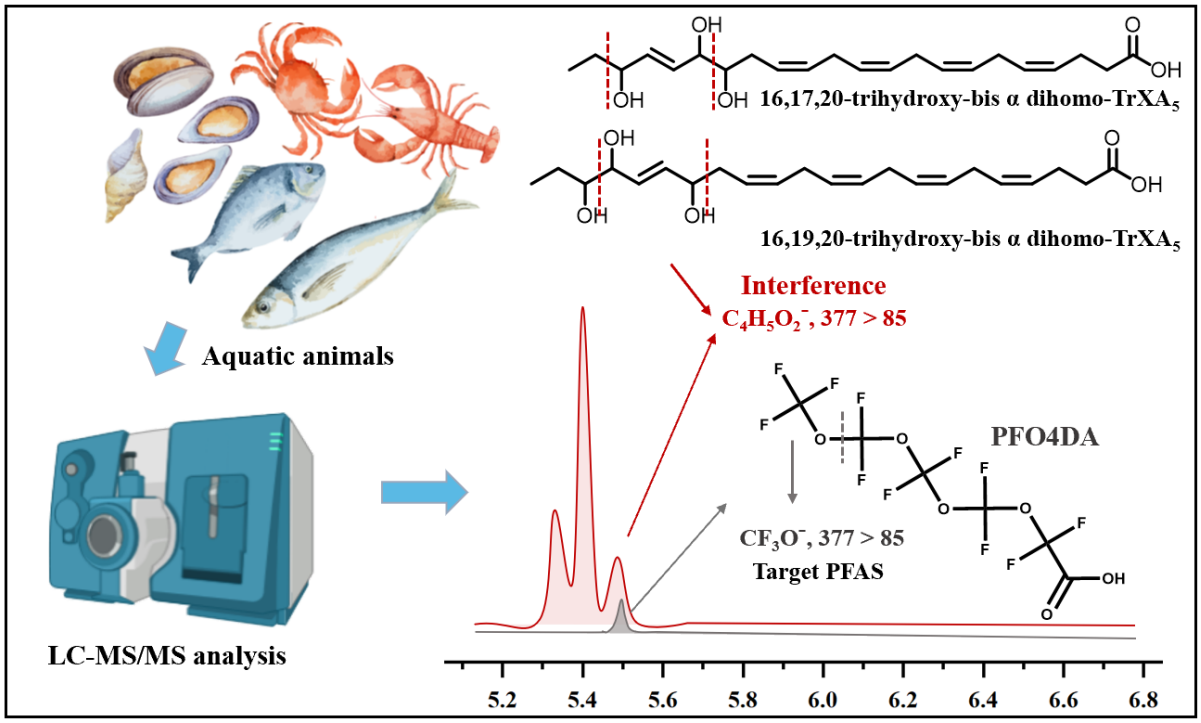
16,17,20-trihydroxy-bis α dihomo-TrXA5
16,19,20-trihydroxy-bis α dihomo-TrXA5
Interference
C4H5O2-, 377 > 85
PFO4DA
CF3O-, 377 > 85
Target PFAS
Aquatic animals
LC-MS/MS analysis
5.2
5.4
5.6
5.8
6.0
6.2
6.4
6.6
6.8

TOC

**ABSTRACT**

Quantitative analyses of per- and polyfluoroalkyl substances (PFAS) commonly rely on low-resolution targeted tandem mass spectrometry (MS/MS) due to its high sensitivity and relatively low operational threshold. Perfluoro-3,5,7,9-butaoxadecanoic acid (PFO4DA), an important constituent of the perfluoropolyether carboxylic acid (PFECA) family, has been widely detected in biotic and abiotic matrices. Nevertheless, marked interference has been observed in the MS/MS transition for PFO4DA (377 > 85) in biological samples, particularly in aquatic organisms, resulting in substantial overestimation of concentrations, reaching up to 66 ng/g. In this study, non-targeted molecular networking strategies, combined with the spectral simulation tools SIRIUS and QCxMS, were applied to identify the source of interference, which was confirmed as an oxygenated metabolite of docosahexaenoic acid (DHA) based on fragmentation patterns matching reference standards. The study further clarified that fatty acids generated the fragment ion $[C_4H_5O_2]^-$ (85.0296 Da), which overlapped with the $[CF_3O]^-$ (84.9907 Da) ion of PFECA compounds under low-resolution conditions, causing signal interference. Analysis of river water and fish samples revealed that this interference had led to a 24-fold overestimation of PFO4DA bioaccumulation in aquatic organisms. These findings are essential for improving the selectivity of environmental exposure assessments for PFECA compounds.

**Keywords**: per- and polyfluoroalkyl substances, perfluoro-3,5,7,9-butaoxadecanoic acid, tandem mass spectrometry, high-resolution mass spectrometry, interference, oxylipin, docosahexaenoic acid.

**Synopsis:** The study employed various non-targeted tools to identify DHA metabolites interfering with PFECA quantification and reported corrected bioaccumulation potential for PFO4DA.

## INTRODUCTION

Per- and polyfluoroalkyl substances (PFAS) represent a diverse class of chemicals characterized by the presence of at least one fully fluorinated methyl or methylene carbon atom.[1] Their exceptional hydrophobic, oleophobic, and thermal stability properties have led to their extensive use in industrial applications and consumer products.[2,3] However, these same properties contribute to their environmental persistence and raise serious toxicological concerns, driving research into their detection in environmental matrices and their potential impact on wildlife and human health.[4–6]

Liquid chromatography coupled with tandem mass spectrometry (LC-MS/MS) analysis using low resolution triple quadrupole mass spectrometry (MS) remains the predominant tool for PFAS quantification. Compared to high-resolution MS, low-resolution MS offers superior sensitivity and precision for targeted analysis and is favored for its lower operational complexity.[7,8] Nevertheless, its limited resolution poses significant analytical challenges when analyzing complex biological matrices, resulting in the inability to effectively differentiate ions with similar m/z ratios, potentially introducing biases in quantification.[9] Bangma et al. compiled the PFAS Interferents List (doi:10.18434/mds2-3040) to emphasize the analytical challenges posed by bile acids and fatty acids that interfere with PFOS, PFHxS, and PFBA detection in biological samples, such as serum and placenta, highlighting liquid chromatography as a solution for resolving overlapping peaks and mitigating interference.[9–11] The PFAS Interferents List is a publicly available and continually updated repository for those working on PFAS low resolution analysis. While progress has been made in addressing interference for legacy PFAS, less is known about emerging PFAS compounds. Many of these compounds, not included in current interference databases, are potentially susceptible to analytical biases due to their distinct structural features. The prevalence of these compounds, their susceptibility to interference, and strategies to mitigate such challenges remain poorly understood, necessitating further investigation into their detection and characterization.

Perfluoropolyether carboxylic acids (PFECA), introduced as novel alternatives to PFOA, have been extensively detected in environmental and biological matrices.[12–14] Despite their widespread detection,

emerging evidence has cast doubt on the concentration accuracy of certain PFECAs. In 2020, Kotlarz et al. reported concentrations of several PFECAs in human serum, but later revised these values after identifying matrix interference during the detection of PFO5DoA.[15] Similarly, during our 2023 study on the biomagnification of PFECAs in the marine food web, we noted considerable asymmetry in chromatographic peaks during the PFO4DA quantification transition (377 > 85) and unusually elevated concentrations of PFO4DA in aquatic organisms, ranging from 2.93 to 80.54 ng/g. These findings indicated the presence of interference, necessitating the exclusion of compromised data from our analysis.[16,17] Subsequent studies have confirmed the presence of similar interference across diverse biological matrices. Given the emerging profile of PFO4DA as a PFAS of concern, particularly due to its potential for bioaccumulation, achieving accurate quantification in biological samples is crucial.[16,17] Building on this, this study sought to identify the source and chemical nature of the PFO4DA interference using high-resolution MS and analysis of its MS/MS fragmentation pathways. These findings pave the way for developing further strategies to enhance the selectivity of PFO4DA quantification and serve as cautionary notes for future studies on similar matrices.

## METHODS AND MATERIALS

**Quantitative assessment by low resolution LC-MS/MS.** A total of 117 biological samples, including plant, animal, and human samples, along with two river surface water samples, were analyzed in this study (details in Table S1) using previously established methods.[16,17] The PFO4DA standard was synthesized in-house, with method provided in SI. Quantitation of PFO4DA was performed using ultra-high-performance liquid chromatography (UHPLC, Exion LC, SCIEX, MA, USA) coupled with triple quadrupole MS (QTRAP 6500 plus, SCIEX, MA, USA). Additional parameters pertaining to the LC gradient and MS parameters are presented in Table S2.

**High-resolution LC-MS/MS analysis.** High-resolution MS data were obtained using the Vanquish Flex UHPLC system coupled with Orbitrap Exploris 120 MS (ThermoFisher, MA, USA).

Chromatographic conditions were identical to those used in quantitative analysis, employing the same column and mobile phase conditions. Further details on instrumentation are provided in Table S3.

**Data Processing and Analysis.** Structural investigation of suspect spectra was conducted through multiple approaches, including the Metfrag Web Tool,[18] QCxMS,[19,20] and SIRIUS,[21] running on several databases, including PubChem,[22] MassBank (massbank.eu),[23] HMDB (hmdb.ca),[24] and GNPS (gnps.ucsd.edu).[25] The maximum mass error threshold for both parent ion searches and fragment candidate analysis were set to 5 ppm. Additionally, seven $F_{4t}$-NeuroP standards were chemically synthesized at the IBMM laboratory.[26–28] Each standard solution was diluted to a concentration of 1 µg/mL with methanol and analyzed under the same parameters detailed in Table S3. Retention times (RT) and MS/MS spectra for these standards were obtained under the same experimental conditions as the samples (Table S4). . The parameters used for molecular networking analysis are detailed in Table S5, and all the raw and processed data are available in the Zenodo dataset (DOI: 10.5281/zenodo.14226855).

## RESULTS AND DISCUSSION

Under high-resolution MS, both PFO4DA standards and biological samples demonstrated symmetrical chromatographic peaks, with an RT of 5.48 min (Figure S1 and Figure S2). To simulate the chromatographic conditions observed under low-resolution MS, all presumptive peaks within an RT range of 5.18–5.78 min and a mass deviation of ±0.5 Da (m/z range 376.4525–377.4525) were extracted from two aquatic animal samples (TS1 and TS2), which exhibited unusually high PFO4DA signal intensities. With this RT and mass range, the strongest signal in both samples corresponded to a MS1 chromatographic peak of m/z 377.2335, displaying a peak shape consistent with the 377 > 85 transition observed under low-resolution MS (Figure S1).

The MS2 spectra of m/z 377.2335 at 5.43 min (Figure S3) confirmed the presence of a high intensity fragment at m/z 85.0296, and its contribution to the chromatographic peaks associated with the 377 > 85 transition in low-resolution MS. Notably, the chemical interferent, represented by a chromatographic peak at 5.47 min, coincided with the RT of the expected PFO4DA peak. In samples derived from aquatic organisms, the intensity of all peaks at m/z 377.2333 and 5.47 min reached 9E5, approximately 10-fold higher than that observed in the 1 ppm PFO4DA standard solution (2.71E4).

Initial investigation into the chemical interferent using Metfrag and Sirius v6.07 indicated a molecular formula of $C_{22}H_{34}O_5$ (100% ZODIAC score),[29] indicating a high likelihood toward an oxylipin metabolite or diterpenoid. To further explore this, the high-resolution MS-MS experiments were optimized to enhance oxylipin fragmentation behavior, following the most recent protocols for Orbitrap instruments.[30] These optimized conditions improved MS2 spectral coverage, revealing molecular ions associated with the 377.233 > 85.029 transition in both samples (Figure S3). Notably, at RT of 5.47 min, molecular ions exhibited MS2 spectra with four prominent fragments: m/z 85.0296, m/z 153.0923, m/z 193.1236, and m/z 233.1547. Further annotation using *CSI:FingerID* in Sirius v6.07 highlighted a strong likelihood of the interferent being derived from docosahexaenoic acid (DHA),[31] with oxylipins ranking among the top 10 candidates. However, library matching confirmed that the chemical interferent was not a neuroprostane derivative (Figure S4-S10). Molecular networking has recently demonstrated exceptional capability in the dereplication and annotation of oxylipins and their non-enzymatic oxidation products, collectively known as non-enzymatic oxidized polyunsaturated fatty acids (NEO-PUFAs).[30,32] Molecular networking analysis was conducted using the GNPS (https://gnps.ucsd.edu)[25] on the two test samples in addition to the MS2 data generated from the *in-vitro* oxidation of DHA with a free radical generator from the Elloumi et. al.[30] (details in Table S5).

Direct matching of the chromatographic feature at RT 5.43 min from samples TS1 and TS2 with nodes in the DHA in vitro oxidation dataset suggested DHA as the biosynthetic precursor from this potential enzymatic or non-enzymatic metabolite (Figure S11). The second candidate identified by Sirius corresponded to a trioxilin from the 5-series (derived from of DHA) ($TrXA_5$), first reported in 1997 and annotated by gas chromatography-electron ionization MS-MS (GC-EI-MS-MS) after derivatization in the rat pineal gland.[33,34] However, no MS2 data under negative collision-induced dissociation (CID) were reported.

Interestingly, Sirius fragment analysis identified the m/z 85.0296 ion (anion $C_4H_5O_2$, 1.1 ppm) as fragment of the omega-terminal, specifically $CH(CH_2)_2COO$-. If accurate, it would be recurrent in oxylipins, and it is not. Another plausible explanation is that the $C_4H_5O_2$ anion arises as 4-hydroxybuta-1,3-dien-1-olate, generated from the fragmentation of pent-3-ene-1,2,5-triol unit characteristic of the

TrXA derivatives. Two HRMS/MS data of TrXA could be retrieved from the GNPS library; 9S,12S,13S-trihydroxy-10E,15Z-octadecadienoic acid (9(S),12(S),13(S)-TriHODE) and 9S,10S,13S-trihydroxy-11E-octadecenoic acid (9(S),10(S),13(S)-TriHOME (Figure S13), the latter only showing m/z 85.0286 (10 ppm) as a main fragment.

To experimentally validate this hypothesis, a commercially available mixture of two hepoxilin A3 ($HXA_3$) ester epimers was hydrolyzed under conditions provided by the supplier (Cayman, MI, USA). This reaction was designed to generate HXA3 free acid while simultaneously inducing epoxide ring opening to yield the required pent-3-ene-1,2,5-triol with two adjacent allylic functions (Figure 1a). High-resolution LC-MS-MS under identical conditions confirmed $HXA_3$ as the major product at m/z 335.222 (Figure S12). Two additional features at m/z 353.22 (+16 amu, 10% relative intensity to HXA3) exhibited MS2 spectra containing two prominent fragment ions: m/z 127.0764 ($C_7H_{11}O_2$, an omega-terminal fingerprint also present in $HXA_3$) and m/z 85.0296 (not present in $HXA_3$). This result is in favor of the production of trioxilin A3 ($TrXA_3$), a well-documented compound, albeit lacking MS2 data in negative CID mode, and established m/z 85.0296 as a distinct fingerprint for the pent-3-ene-1,2,5-triol unit in trioxilin of the A type with at least one double bond in allylic position of the triol unit.

Further validation of the origin of the m/z 85.0296 fragment was performed using quantum-chemistry CID-MS with QCxMS software.[19] Oxylipins are particularly reluctant at providing pertinent in silico MSMS simulation, probably due to the so-called mobile-proton effect as the pertinent molecular ions (deprotomers) during the CID process may be delicate to ascertain.[35,36] Initial fragmentation modeling was performed with TrXA3 structures, affording reasonable MSMS fragments and confirming the expected origin of the m/z 85.0296 ion (Figure 1a, and Figure S14) as 4-hydroxybuta-1,3-dien-1-olate. Hence, simulations also revealed that reversing the sequence of the triol unit produced similar fragmentation behaviors. Subsequently simulations of all possible 10 isomers of the 5-series ($TrXA_5$) were attempted with random attribution of the stereocenters (Figure 1b). All simulations did generate m/z 85.0296 with high statistics (indistinctively of the several deprotomers per $TrXA_5$) clearly confirming it as a fingerprint. Two of the $TrXA_5$ derived from the hydroperoxide precursor 13- and 17-HpDHA seem pertinent as candidates as the four primary fragments could be retrieved in high intensity

158 (albeit the m/z 193 for the former, and m/z 153 for the latter). MS3 investigation revealed that the four
159 main fragments are not consecutive ions. A breakthrough came from the detailed insights into the
160 fragmentation pathways leading to the four main fragments with QCxMS software showing that m/z
161 153.0923 to the contrary of m/z 193.1234 and m/z 233.1547 are from two different part of the molecule
162 in the case of TrXA5(originating from 13- and 17-HpDHA (Figure S15). Indeed, a second molecular
163 network between chemical interferent spectra and an oxylipin analog of +2 Da revealed that +2 Da is
164 also added to the three main fragments (except m/z 85.02; Figure S16). This finding has to rule out the
165 TrXA5 from 13- and 17-HpDHA as the chemical interferent because+2 Da should not have added to
166 m/z 153.0923 fragment. If one would conclude on our study on the fragmentation pathways leading to
167 the main fragments in all simulations and the second molecular network, the outcome would be that the
168 chemical interferent is from 16- and 20–HpDHA. As the best of our knowledge, only they could lead to
169 such additional +2 Da fragments from the same part of the molecule. One explanation for the failure in
170 quantum simulation for those remaining $TrXA_5$ structures is accounting for their particular
171 isomerization potential (three skipped diene units) resulting in wrong initial deprotomers or excessive
172 isomerization before fragmentation. We then proposed the chemical interferent structure be either
173 16,17,20-trihydroxy bis α dihomo-$TrXA_5$ or 16,19,20-trihydroxy-trihydroxy bis α dihomo-$TrXA_5$
174 without possible further chemical distinction at present.

175

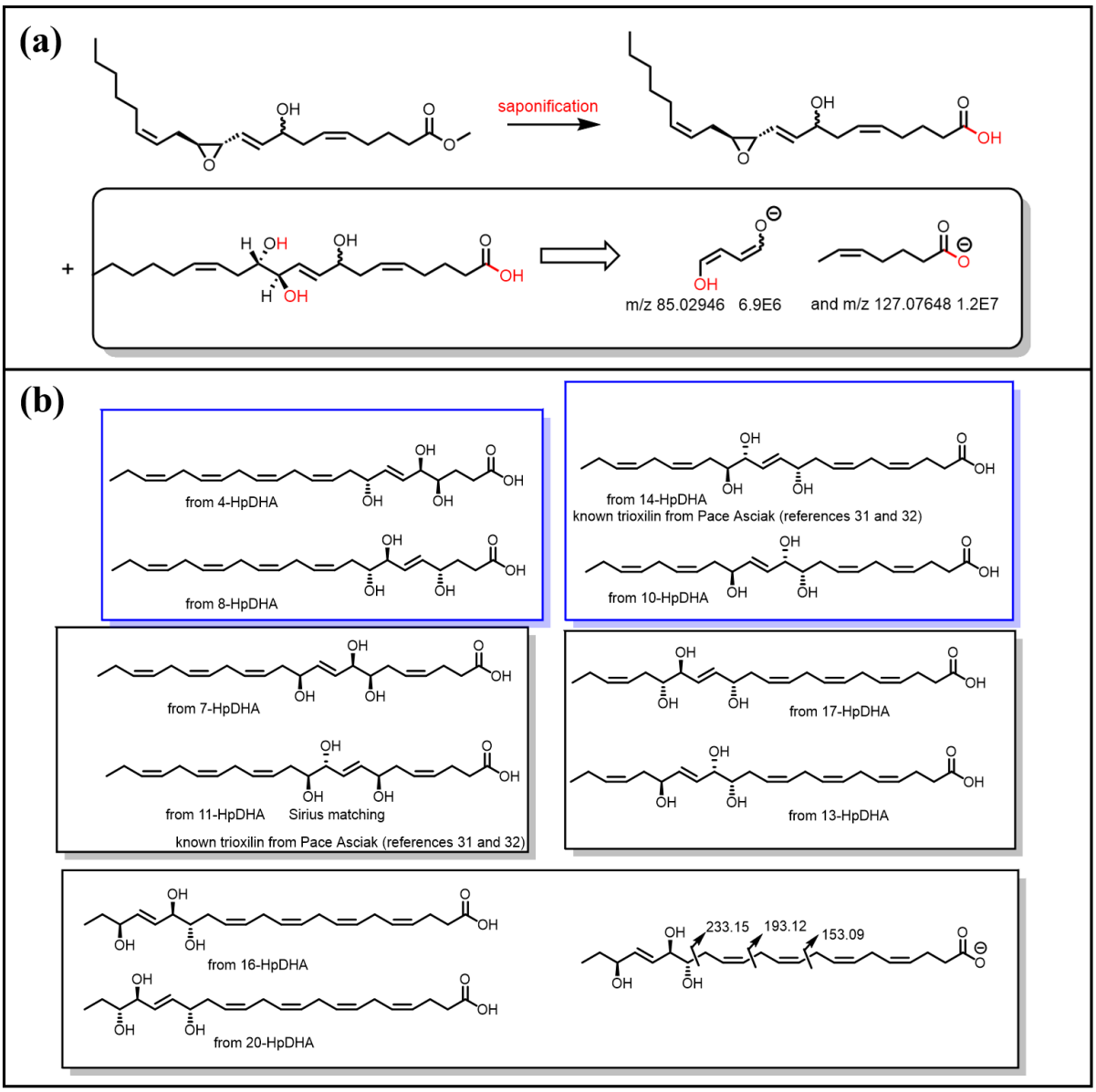


**Figure 1.** (a) Saponification of HXA3 ester and MSMS main fragments of free HXA3. (b) List of the 10 TrXA5 simulated by quantum chemical mass spectrometry with QCxMS, and two most probable structures of the chemical interferent.

Analysis of high- and low-resolution MS data revealed that interference was exclusively detected in animal-derived samples, with varying levels observed across livestock, poultry, and human cord blood. Aquatic organisms exhibited particularly pronounced interference intensities. In contrast, no interference was detected in vegetables, milk, eggs, or breast milk, suggesting that the interfering substance may be an animal-specific metabolic product. This hypothesis aligns with the likely involvement of DHA as a precursor. Given that the m/z 85 fragment is highly susceptible to interference

by the aforementioned fatty acids under low-resolution MS conditions, the m/z 151 fragment ($CF_3OCF_2O$-) was selected as the quantification fragment. By comparing the intensity ratios of the two transitions, the extent of interference across different samples was estimated (Figure 2a). Notably, aquatic organisms exhibited the most pronounced interference, with deviations from actual concentrations ranging from 4.02- to 150.68-fold. Absolute deviations in concentration ranged from 2.18 to 65.69 ng/g. To account for the interference, bioaccumulation factor (BAF) values were recalculated for river water samples from two locations and 10 crucian carp specimens (Table S6). The corrected BAF values, presented in Figure 2b, were significantly lower following interference elimination, decreasing from 206.80 L/kg to 8.75 L/kg. These findings underscore the substantial impact of interfering substances on overestimating the bioconcentration potential of PFO4DA, highlighting the importance of refining analytical methods to achieve accurate quantification.

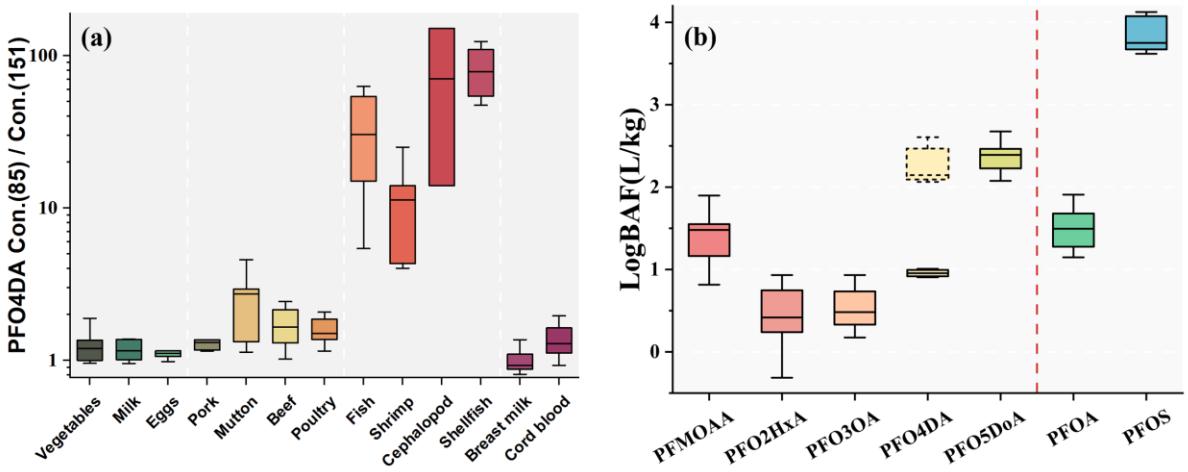


**Figure 2.** (a) Extent of interference in PFO4DA concentrations across environmental samples. Con.(85) and Con.(151) represent the concentrations quantified using the transitions 377 > 85 and 377 > 151, respectively. (b) Corrected BAF values of PFO4DA and other PFAS after adjusting for interference. Boxes drawn with dashed lines represent data prior to interference elimination. (PFMOAA, PFO2HxA, PFO3OA, and PFO5DoA are homologs of PFO4DA, differing by $CF_2O$ units, with carbon chain lengths ranging from 2 to 6)

Fatty acid metabolites are a well-documented source of interference in PFAS detection. For instance, 3-oxo-dodecanoic acid has been shown to interfere with the 213 > 169 transition of PFBA in placental samples.[10] Similarly, potential interference has been identified in PFPeA detection in shellfish and cocoa mix samples, with endogenous steroid sulfates disrupting PFHxS detection in human serum and

taurodeoxycholic acid interfering with PFOS detection in biological tissues and eggs.[9,11,37,38] Our study focused on PFO4DA, a member of the PFECA class, which includes structurally related congeners such as PFMOAA, PFO2HxA, and PFO3OA. These PFECA compounds, differentiated by $CF_2$ or $OCF_2$ units, represent an emerging and significant subclass of PFAS, driving extensive biomonitoring efforts due to their environmental prevalence.

The primary fragment observed for PFECAs in MS analysis is $[CF_3O]$-, corresponding to the m/z 85 ion, with no other significant fragments exceeding a relative intensity of 10% (Figure S3). Furthermore, $[CF_3O]$- is not capable of further fragmentation within the mass spectrometer, making the m/z 85 fragment the predominant marker for quantifying PFECAs. However, the trihydroxy unsaturated structural motif identified in this study fragments to produce $[C_4H_5O_2]$-, introducing substantial interference during low-resolution MS analysis. This study highlighted the potential for similar fatty acid structures to disrupt the quantification of other PFECAs. By clarifying the fragmentation mechanisms responsible for this interference, the findings offer critical guidance for researchers quantifying PFECAs in environmental matrices. The study also emphasizes the need for caution when interpreting data, as such interference could lead to significant overestimations of PFAS levels. Although alternative mass transitions and high-resolution MS can mitigate interference, both approaches often reduce sensitivity compared to conventional detection methods. Consequently, further refinement of analytical techniques is essential to enhance PFECA quantification. It is important to note that when selecting alternative transitions for quantifying PFECA, transitions 377>153 and 377>193 should be avoided, as they are also present in interfering substances. Conversely, these transitions can be utilized to monitor whether the quantification process is affected by interference.

This study identified potential interference in the PFO4DA transition during biological sample analysis, likely attributed to a non-enzymatic oxygenated metabolite of DHA. The fragmentation mechanisms of the interfering structure were elucidated, enabling a deeper understanding of its impact on quantification. As a prominent member of the PFECA class, PFO4DA represents a significant environmental contaminant, with potential health risks associated with high exposure levels. As such, precise quantification is essential for evaluating toxicological risks, characterizing environmental behaviors,

and conducting health risk assessments. The findings and methodologies presented in this study provide a critical framework for identifying and mitigating quantification issues associated with PFECAs in biological matrices. By addressing potential sources of interference, this work aims to improve the accuracy of PFAS quantification, reduce the likelihood of overestimation, and enhance the reliability of future research in this field.

**Supporting Information**

Information on raw files of tested samples, detailed instrumental analysis methods, relevant MS/MS spectra and details of the molecular networking approach can be found in the Supporting Information.

**Acknowledgments**

This study was supported by the National Key Research and Development Program of China (2022YFC3105700) and National Natural Science Foundation of China (22322607, 22276124). JMG would like to express our gratitude to the National Research Agency, under the acronym TA-BOOm [ANR-20-CE44-0001], for funding and supporting molecular networking work, as well as to LabCom OxyBleu-MARI [ANR-22-LCV1-0007] and CNRS for the 80|Prime project [INSB-INC-80PRIME]. ASI acknowledges the JDC2022-049354-I grant funded by MCIN/AEI/10.13039/501100011033 and "European Union NextGenerationEU/PRTR", and the CIGE/2022/107 research project from *Generalitat Valenciana,* Conselleria d'Educació, Cultura, Universitats i Ocupació. We gratefully acknowledge the *Servei d'Informàtica* of the Universitat de València for providing access to the LluisVives v2 HPC cluster and their technical support.

## REFERENCES


(1) Evich, M. G.; Davis, M. J. B.; McCord, J. P.; Acrey, B.; Awkerman, J. A.; Knappe, D. R. U.; Lindstrom, A. B.; Speth, T. F.; Tebes-Stevens, C.; Strynar, M. J.; Wang, Z.; Weber, E. J.; Henderson, W. M.; Washington, J. W. Per- and Polyfluoroalkyl Substances in the Environment. *Science 375* (6580), eabg9065. https://doi.org/10.1126/science.abg9065.

(2) Glüge, J.; Scheringer, M.; Cousins, I. T.; DeWitt, J. C.; Goldenman, G.; Herzke, D.; Lohmann, R.; Ng, C. A.; Trier, X.; Wang, Z. An Overview of the Uses of Per- and Polyfluoroalkyl Substances (PFAS). *Env. Sci Process. Impacts* **2020**, *22* (12), 2345–2373. https://doi.org/10.1039/D0EM00291G.

(3) Gaines, L. G. T. Historical and Current Usage of Per- and Polyfluoroalkyl Substances (PFAS): A Literature Review. *Am. J. Ind. Med.* **2023**, *66* (5), 353–378. https://doi.org/10.1002/ajim.23362.

(4) De Silva, A. O.; Armitage, J. M.; Bruton, T. A.; Dassuncao, C.; Heiger-Bernays, W.; Hu, X. C.; Kärrman, A.; Kelly, B.; Ng, C.; Robuck, A.; Sun, M.; Webster, T. F.; Sunderland, E. M. PFAS Exposure Pathways for Humans and Wildlife: A Synthesis of Current Knowledge and Key Gaps in Understanding. *Environ. Toxicol. Chem.* **2021**, *40* (3), 631–657. https://doi.org/10.1002/etc.4935.

(5) Ng, C.; Cousins, I. T.; DeWitt, J. C.; Glüge, J.; Goldenman, G.; Herzke, D.; Lohmann, R.; Miller, M.; Patton, S.; Scheringer, M.; Trier, X.; Wang, Z. Addressing Urgent Questions for PFAS in the 21st Century. *Environ. Sci. Technol.* **2021**, *55* (19), 12755–12765. https://doi.org/10.1021/acs.est.1c03386.

(6) Sunderland, E. M.; Hu, X. C.; Dassuncao, C.; Tokranov, A. K.; Wagner, C. C.; Allen, J. G. A Review of the Pathways of Human Exposure to Poly- and Perfluoroalkyl Substances (PFASs) and Present Understanding of Health Effects. *J. Expo. Sci. Environ. Epidemiol.* **2019**, *29* (2), 131–147. https://doi.org/10.1038/s41370-018-0094-1.

(7) Shen, Y.; Wang, L.; Ding, Y.; Liu, S.; Li, Y.; Zhou, Z.; Liang, Y. Trends in the Analysis and Exploration of Per- and Polyfluoroalkyl Substances (PFAS) in Environmental Matrices: A Review. *Crit. Rev. Anal. Chem.* **2024**, *54* (8), 3171–3195. https://doi.org/10.1080/10408347.2023.2231535.

(8) Jia, S.; Marques Dos Santos, M.; Li, C.; Snyder, S. A. Recent Advances in Mass Spectrometry Analytical Techniques for Per- and Polyfluoroalkyl Substances (PFAS). *Anal. Bioanal. Chem.* **2022**, *414* (9), 2795–2807. https://doi.org/10.1007/s00216-022-03905-y.

(9) Bangma, J.; Barry, K. M.; Fisher, C. M.; Genualdi, S.; Guillette, T. C.; Huset, C. A.; McCord, J.; Ng, B.; Place, B. J.; Reiner, J. L.; Robuck, A.; Rodowa, A. E. PFAS Ghosts: How to Identify, Evaluate, and Exorcise New and Existing Analytical Interference. *Anal. Bioanal. Chem.* **2024**, *416* (8), 1777–1785. https://doi.org/10.1007/s00216-024-05125-y.

(10) Bangma, J. T.; Reiner, J.; Fry, R. C.; Manuck, T.; McCord, J.; Strynar, M. J. Identification of an Analytical Method Interference for Perfluorobutanoic Acid in Biological Samples. *Environ. Sci. Technol. Lett.* **2021**, *8* (12), 1085–1090. https://doi.org/10.1021/acs.estlett.1c00901.

(11) Bangma, J.; McCord, J.; Giffard, N.; Buckman, K.; Petali, J.; Chen, C.; Amparo, D.; Turpin, B.; Morrison, G.; Strynar, M. Analytical Method Interferences for Perfluoropentanoic Acid (PFPeA) and Perfluorobutanoic Acid (PFBA) in Biological and Environmental Samples. *Chemosphere* **2023**, *315*, 137722. https://doi.org/10.1016/j.chemosphere.2022.137722.

(12) Yao, J.; Pan, Y.; Sheng, N.; Su, Z.; Guo, Y.; Wang, J.; Dai, J. Novel Perfluoroalkyl Ether

Carboxylic Acids (PFECAs) and Sulfonic Acids (PFESAs): Occurrence and Association with Serum Biochemical Parameters in Residents Living Near a Fluorochemical Plant in China. *Environ. Sci. Technol.* **2020**, *54* (21), 13389–13398. https://doi.org/10.1021/acs.est.0c02888.

(13) Yao, J.; Pan, Y.; Huan, Y.; Dai, J. Occurrence of Novel Perfluoroalkyl Ether Carboxylic Acids in River Water and Human Urine Quantified by a Simple Liquid–Liquid Microextraction Approach Coupled with LC–MS/MS. *Environ. Sci. Technol. Lett.* **2021**, *8* (9), 773–778. https://doi.org/10.1021/acs.estlett.1c00563.

(14) Chen, Z.; Zhan, X.; Zhang, J.; Diao, J.; Su, C.; Sun, Q.; Zhou, Y.; Zhang, L.; Bi, R.; Ye, M.; Wang, T. Bioaccumulation and Risk Mitigation of Legacy and Novel Perfluoroalkyl Substances in Seafood: Insights from Trophic Transfer and Cooking Method. *Environ. Int.* **2023**, *177*, 108023. https://doi.org/10.1016/j.envint.2023.108023.

(15) Kotlarz, N.; McCord, J.; Wiecha, N.; Weed, R. A.; Cuffney, M.; Enders, J. R.; Strynar, M.; Knappe, D. R. U.; Reich, B. J.; Hoppin, J. A. Reanalysis of PFO5DoA Levels in Blood from Wilmington, North Carolina, Residents, 2017–2018. *Environ. Health Perspect.* **2024**, *132* (2), 027701. https://doi.org/10.1289/EHP13339.

(16) Li, Y.; Yao, J.; Zhang, J.; Pan, Y.; Dai, J.; Ji, C.; Tang, J. First Report on the Bioaccumulation and Trophic Transfer of Perfluoroalkyl Ether Carboxylic Acids in Estuarine Food Web. *Environ. Sci. Technol.* **2022**, *56* (10), 6046–6055. https://doi.org/10.1021/acs.est.1c00965.

(17) Li, Y.; Yao, J.; Pan, Y.; Dai, J.; Tang, J. Trophic Behaviors of PFOA and Its Alternatives Perfluoroalkyl Ether Carboxylic Acids (PFECAs) in a Coastal Food Web. *J. Hazard. Mater.* **2023**, *452*, 131353. https://doi.org/10.1016/j.jhazmat.2023.131353.

(18) Ruttkies, C.; Schymanski, E. L.; Wolf, S.; Hollender, J.; Neumann, S. MetFrag Relaunched: Incorporating Strategies beyond in Silico Fragmentation. *J. Cheminformatics* **2016**, *8* (1), 3. https://doi.org/10.1186/s13321-016-0115-9.

(19) Koopman, J.; Grimme, S. From QCEIMS to QCxMS: A Tool to Routinely Calculate CID Mass Spectra Using Molecular Dynamics. *J. Am. Soc. Mass Spectrom.* **2021**, *32* (7), 1735–1751. https://doi.org/10.1021/jasms.1c00098.

(20) Koopman, J.; Grimme, S. Calculation of Mass Spectra with the QCxMS Method for Negatively and Multiply Charged Molecules. *J. Am. Soc. Mass Spectrom.* **2022**, *33* (12), 2226–2242. https://doi.org/10.1021/jasms.2c00209.

(21) Dührkop, K.; Fleischauer, M.; Ludwig, M.; Aksenov, A. A.; Melnik, A. V.; Meusel, M.; Dorrestein, P. C.; Rousu, J.; Böcker, S. SIRIUS 4: A Rapid Tool for Turning Tandem Mass Spectra into Metabolite Structure Information. *Nat. Methods* **2019**, *16* (4), 299–302. https://doi.org/10.1038/s41592-019-0344-8.

(22) Kim, S.; Thiessen, P.; Bolton, E.; Chen, J.; Fu, G.; Gindulyte, A.; Han, L.; He, J.; Shoemaker, B.; Wang, J.; Yu, B.; Zhang, J.; Bryant, S. PubChem Substance and Compound Databases. *Nucleic Acids Res.* **2015**, *44*. https://doi.org/10.1093/nar/gkv951.

(23) Horai, H.; Arita, M.; Kanaya, S.; Nihei, Y.; Ikeda, T.; Suwa, K.; Ojima, Y.; Tanaka, K.; Tanaka, S.; Aoshima, K.; Oda, Y.; Kakazu, Y.; Kusano, M.; Tohge, T.; Matsuda, F.; Sawada, Y.; Hirai, M. Y.; Nakanishi, H.; Ikeda, K.; Akimoto, N.; Maoka, T.; Takahashi, H.; Ara, T.; Sakurai, N.; Suzuki, H.; Shibata, D.; Neumann, S.; Iida, T.; Tanaka, K.; Funatsu, K.; Matsuura, F.; Soga, T.; Taguchi, R.; Saito, K.; Nishioka, T. MassBank: A Public Repository for Sharing Mass Spectral Data for Life Sciences. *J. Mass Spectrom.* **2010**, *45* (7), 703–714.

https://doi.org/10.1002/jms.1777.
(24) Wishart, D. S.; Feunang, Y. D.; Marcu, A.; Guo, A. C.; Liang, K.; Vázquez-Fresno, R.; Sajed, T.; Johnson, D.; Li, C.; Karu, N.; Sayeeda, Z.; Lo, E.; Assempour, N.; Berjanskii, M.; Singhal, S.; Arndt, D.; Liang, Y.; Badran, H.; Grant, J.; Serra-Cayuela, A.; Liu, Y.; Mandal, R.; Neveu, V.; Pon, A.; Knox, C.; Wilson, M.; Manach, C.; Scalbert, A. HMDB 4.0: The Human Metabolome Database for 2018. *Nucleic Acids Res.* **2018**, *46* (D1), D608–D617. https://doi.org/10.1093/nar/gkx1089.
(25) Aron, A. T.; Gentry, E. C.; McPhail, K. L.; Nothias, L.-F.; Nothias-Esposito, M.; Bouslimani, A.; Petras, D.; Gauglitz, J. M.; Sikora, N.; Vargas, F.; van der Hooft, J. J. J.; Ernst, M.; Kang, K. B.; Aceves, C. M.; Caraballo-Rodríguez, A. M.; Koester, I.; Weldon, K. C.; Bertrand, S.; Roullier, C.; Sun, K.; Tehan, R. M.; Boya P., C. A.; Christian, M. H.; Gutiérrez, M.; Ulloa, A. M.; Tejeda Mora, J. A.; Mojica-Flores, R.; Lakey-Beitia, J.; Vásquez-Chaves, V.; Zhang, Y.; Calderón, A. I.; Tayler, N.; Keyzers, R. A.; Tugizimana, F.; Ndlovu, N.; Aksenov, A. A.; Jarmusch, A. K.; Schmid, R.; Truman, A. W.; Bandeira, N.; Wang, M.; Dorrestein, P. C. Reproducible Molecular Networking of Untargeted Mass Spectrometry Data Using GNPS. *Nat. Protoc.* **2020**, *15* (6), 1954–1991. https://doi.org/10.1038/s41596-020-0317-5.
(26) Oger, C.; Bultel-Poncé, V.; Guy, A.; Balas, L.; Rossi, J.-C.; Durand, T.; Galano, J.-M. The Handy Use of Brown's P2-Ni Catalyst for a Skipped Diyne Deuteration: Application to the Synthesis of a [D4]-Labeled F4t-Neuroprostane. *Chem. – Eur. J.* **2010**, *16* (47), 13976–13980. https://doi.org/10.1002/chem.201002304.
(27) Guy, A.; Oger, C.; Heppekausen, J.; Signorini, C.; De Felice, C.; Fürstner, A.; Durand, T.; Galano, J.-M. Oxygenated Metabolites of N-3 Polyunsaturated Fatty Acids as Potential Oxidative Stress Biomarkers: Total Synthesis of 8-F3t-IsoP, 10-F4t-NeuroP and [D4]-10-F4t-NeuroP. *Chem. – Eur. J.* **2014**, *20* (21), 6374–6380. https://doi.org/10.1002/chem.201400380.
(28) Guy, A. M., Jérémy; Degrange, Thomas; Reversat, Guillaume; Bultel-Poncé, Valérie; Durand, Thierry; Galano, Jean-Marie; Oger, Camille. Total Synthesis of DHA and DPAn-3 Non-Enzymatic Oxylipins. *Synthesis* **2021**, *54* (05), 1431–1445. https://doi.org/10.1055/a-1654-4111.
(29) Ludwig, M.; Nothias, L.-F.; Dührkop, K.; Koester, I.; Fleischauer, M.; Hoffmann, M. A.; Petras, D.; Vargas, F.; Morsy, M.; Aluwihare, L.; Dorrestein, P. C.; Böcker, S. Database-Independent Molecular Formula Annotation Using Gibbs Sampling through ZODIAC. *Nat. Mach. Intell.* **2020**, *2* (10), 629–641. https://doi.org/10.1038/s42256-020-00234-6.
(30) Elloumi, A.; Mas-Normand, L.; Bride, J.; Reversat, G.; Bultel-Poncé, V.; Guy, A.; Oger, C.; Demion, M.; Le Guennec, J.-Y.; Durand, T.; Vigor, C.; Sánchez-Illana, Á.; Galano, J.-M. From MS/MS Library Implementation to Molecular Networks: Exploring Oxylipin Diversity with NEO-MSMS. *Sci. Data* **2024**, *11* (1), 193. https://doi.org/10.1038/s41597-024-03034-4.
(31) Hoffmann, M. A.; Nothias, L.-F.; Ludwig, M.; Fleischauer, M.; Gentry, E. C.; Witting, M.; Dorrestein, P. C.; Dührkop, K.; Böcker, S. High-Confidence Structural Annotation of Metabolites Absent from Spectral Libraries. *Nat. Biotechnol.* **2022**, *40* (3), 411–421. https://doi.org/10.1038/s41587-021-01045-9.
(32) Watrous, J. D.; Niiranen, T. J.; Lagerborg, K. A.; Henglin, M.; Xu, Y.-J.; Rong, J.; Sharma, S.; Vasan, R. S.; Larson, M. G.; Armando, A.; Mora, S.; Quehenberger, O.; Dennis, E. A.; Cheng, S.; Jain, M. Directed Non-Targeted Mass Spectrometry and Chemical Networking for

Discovery of Eicosanoids and Related Oxylipins. *Cell Chem. Biol.* **2019**, *26* (3), 433-442.e4. https://doi.org/10.1016/j.chembiol.2018.11.015.
(33) Reynaud, D.; Pace-Asciak, C. R. Docosahexaenoic Acid Causes Accumulation of Free Arachidonic Acid in Rat Pineal Gland and Hippocampus to Form Hepoxilins from Both Substrates. *Biochim. Biophys. Acta BBA - Lipids Lipid Metab.* **1997**, *1346* (3), 305–316. https://doi.org/10.1016/S0005-2760(97)00041-6.
(34) Pace-Asciak, C. R. Pathophysiology of the Hepoxilins. *Oxyg. Metab. PUFA Anal. Biol. Relev.* **2015**, *1851* (4), 383–396. https://doi.org/10.1016/j.bbalip.2014.09.007.
(35) Johnson, R. S. Mass Spectrometric Measurement of Changes in Protein Hydrogen Exchange Rates That Result from Point Mutations. *J. Am. Soc. Mass Spectrom.* **1996**, *7* (6), 515–521. https://doi.org/10.1016/1044-0305(96)00009-8.
(36) Csonka, I. P.; Paizs, B.; Lendvay, G.; Suhai, S. Proton Mobility and Main Fragmentation Pathways of Protonated Lysylglycine. *Rapid Commun. Mass Spectrom.* **2001**, *15* (16), 1457–1472. https://doi.org/10.1002/rcm.388.
(37) Benskin, J. P.; Bataineh, M.; Martin, J. W. Simultaneous Characterization of Perfluoroalkyl Carboxylate, Sulfonate, and Sulfonamide Isomers by Liquid Chromatography−Tandem Mass Spectrometry. *Anal. Chem.* **2007**, *79* (17), 6455–6464. https://doi.org/10.1021/ac070802d.
(38) Chan, E.; Sandhu, M.; Benskin, J. P.; Ralitsch, M.; Thibault, N.; Birkholz, D.; Martin, J. W. Endogenous High-performance Liquid Chromatography/Tandem Mass Spectrometry Interferences and the Case of Perfluorohexane Sulfonate (PFHxS) in Human Serum; Are We Overestimating Exposure? *Rapid Commun. Mass Spectrom.* **2009**, *23* (10), 1405–1410. https://doi.org/10.1002/rcm.4012.

# Supporting Information

## (27 pages, 16 figures, 6 tables)

# Annotating DHA Metabolites Interfering with the Quantification of Emerging Perfluoroalkyl Ether Carboxylic Acids

Yuyan Ji[1], Yitao Pan[1*], Jean-Marie Galano[2], Ángel Sánchez-Illana[3], Xinchen Miao[1], Fengfeng Dong[1], Camille Oger[2], Thierry Durand[2], and Jiayin Dai[1]

[1]State Environmental Protection Key Laboratory of Environmental Health Impact Assessment of Emerging Contaminants, School of Environmental Science and Engineering, Shanghai Jiao Tong University, Shanghai 200240, China.

[2]Institut des Biomolécules Max Mousseron (IBMM), Pôle Chimie Balard Recherche, UMR 5247, Université de Montpellier, CNRS, ENSCM, Montpellier, France.

[3]Department of Analytical Chemistry, University of Valencia, Burjassot, Spain.

***Correspondence author:** Yitao Pan, State Environmental Protection Key Laboratory of Environmental Health Impact Assessment of Emerging Contaminants, School of Environmental Science and Engineering, Shanghai Jiao Tong University, 800 Dongchuan Road, Shanghai 200240, China. E-mail: panyitao@sjtu.edu.cn

**Competing financial interests:** The authors declare no conflicts of interest.

# Table of Contents

**Reference Standard Hydrolysis Experiment.**

Reference standard Hepoxilin A3 methyl ester (purity: ≥98%) was purchased from Cayman. Alkaline hydrolysis of HxA3 methyl ester was performed as follows: Prepared a hydrolysis solution consisting of degassed acetone (8 ml) and 0.25 M NaOH (2 ml) and cooled it to 0°C. Evaporated the hexane/1% TEA solution of HxA3 methyl ester just to dryness under nitrogen and immediately added 4 ml of the hydrolysis solution per 1 mg of HxA3 methyl ester. Allowed the reaction to stand under an inert atmosphere of nitrogen or argon at 22°C for 40 minutes. The reaction product was diluted tenfold with water and then subjected to instrumental analysis.

**Files converting method.**

The high-resolution LC-MS/MS rawdata were fist converted to .mzML with ThermoRawFileParser and analyzed with mzmine (version 4.3.0) for the LC-MS1 feature extraction and MS/MS spectra assignment to each feature. The MS/MS spectra were then exported to .mgf files for the GNPS molecular networking approach using NEOMSMS library.

**General information of NMR**

NMR spectra were obtained on a 400 MHz spectrometer using Methanol-d4 or Acetone-d6 as deuterated solvents, with proton and fluorine resonances at 400 MHz and 376 MHz, respectively. Chemical shifts (δ) are reported in ppm and coupling constants (J) are in hertz (Hz). The following abbreviations were used to explain the multiplicities: s = singlet, d = doublet, t = triplet, q = quartet, m = multiplet, br = broad.

**Synthesis of potassium salt**

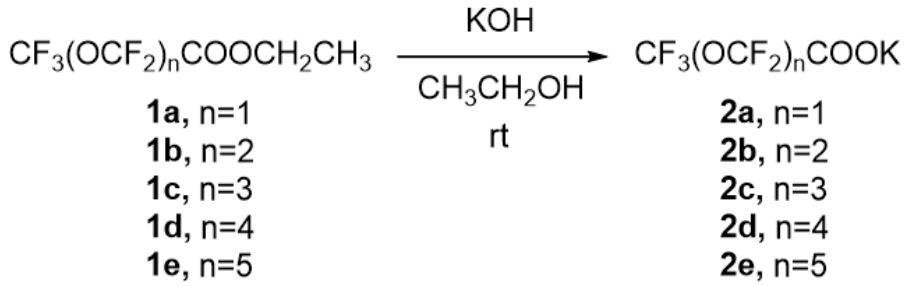


**Typical procedure**

To a 100 mL flask containing a magnetic stirring bar were added ethanol (20 mL), KOH (70 mmol, 7 mol/L) and 1d (100 mmol). The mixture was stirred vigorously at room temperature overnight. Removing the solvent under reduced pressure with a rotary evaporator gave a light yellow gelatinous solid-liquid mixture. After heating at 45 °C under vacuum, a white solid was obtained.

**potassium 1,1,1,3,3,5,5,7,7,9,9-undecafluoro-2,4,6,8-tetraoxadecan-10-oate (2d): $^{19}$F NMR** (376 MHz, Methanol-$d_4$) δ -54.4 – -54.3 (m, 2F), -56.3 – -56.4 (m, 2F), -56.8 – -57.0 (m, 2F), -58.7 (t, $J$ = 9.0 Hz, 3F), -80.7 (t, $J$ = 10.3 Hz, 2F).

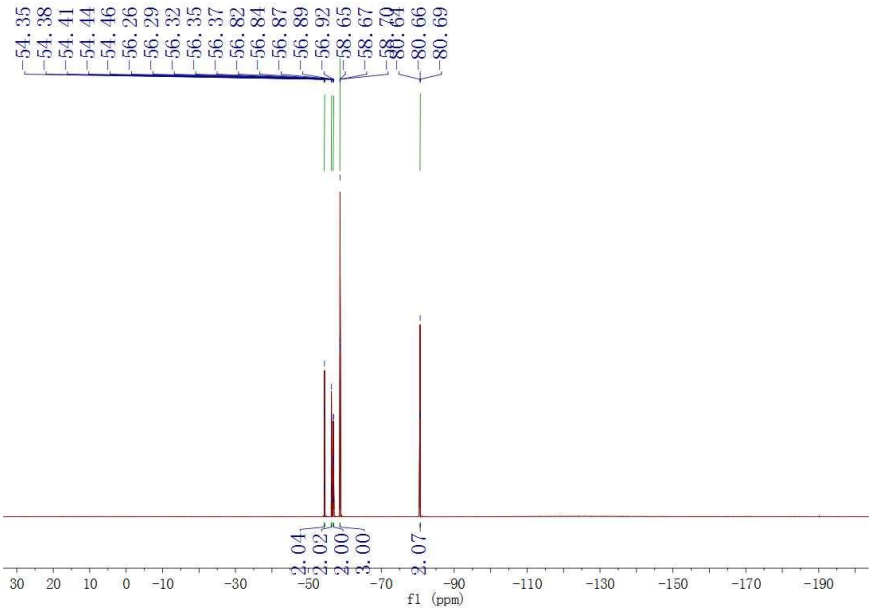


$^{19}$F NMR of **2d** (376 MHz，Acetone-$d_6$)

**Bioaccumulation Factor (BAF) Calculation.**

Two sampling sites were selected, and at each site, 500 mL of surface water and five fish samples were collected. The concentrations of these samples were used to calculate the BAF using the formula below.

$$BAF = \frac{C_o}{C_w}$$

where $C_o$ refers to the PFAS concentration in organisms on the wet weight basis (ng/kg), and $C_w$ is defined as the PFAS concentration in water (ng/L).

**Relative files:**

Raw files and mgf files of tested samples TS1(Q18) and TS2(Q19):

DOI: 10.5281/zenodo.14226855

https://doi.org/10.5281/zenodo.14226855

Dataset of the in vitro oxidation of DHA (oxDHA) and other oxylipins extracts:

https://zenodo.org/records/8345059

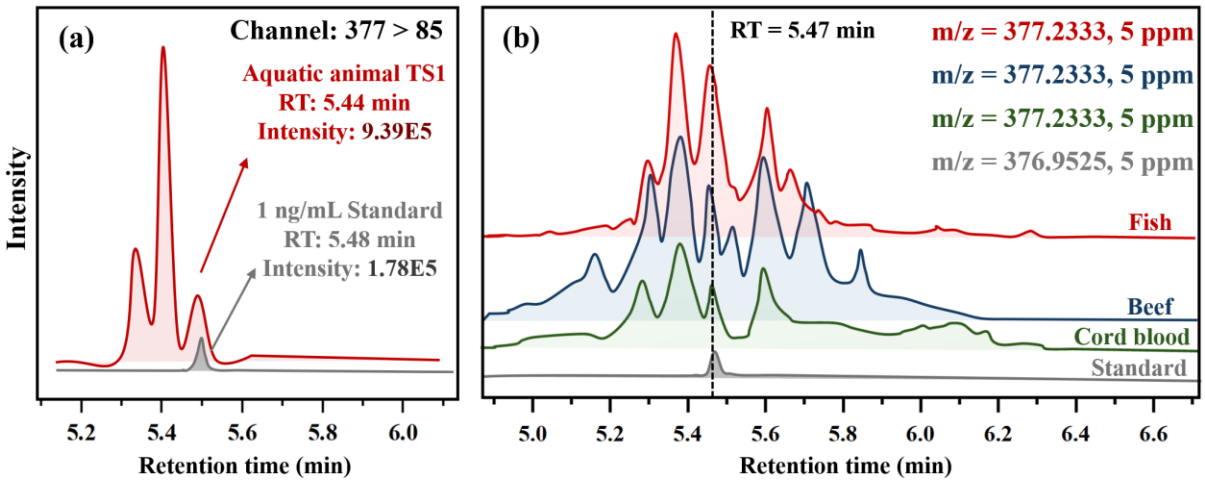


**Figure S1.** (a) Extracted Ion Chromatograms (EICs) of aquatic animal tested sample TS1 and 1 ng/mL PFO4DA standard in 377 > 85 transition under low-resolution MS. (b) EICs for m/z 377.2333 in different biological samples and m/z 376.9525 in 1 ng/mL PFO4DA standard under a 5-ppm mass error in high-resolution MS.

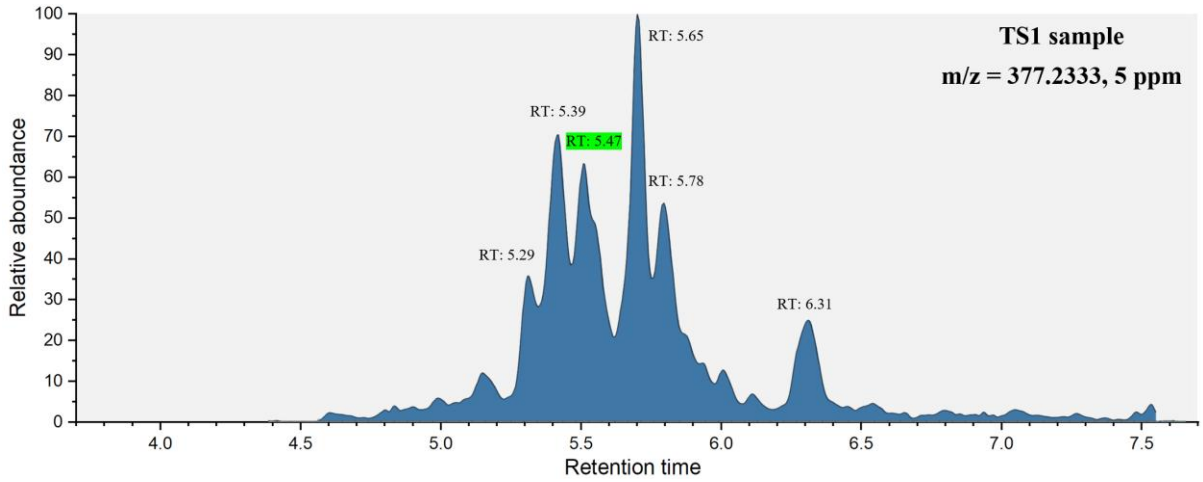


**Figure S2.** Extracted Ion Chromatograms (EICs) of the interference peak at m/z = 377.2333, retention time = 5.47 under high-resolution mass spectrometry. Detailed LC and HRMS parameters can be found in Tables S2 and S3, respectively.·

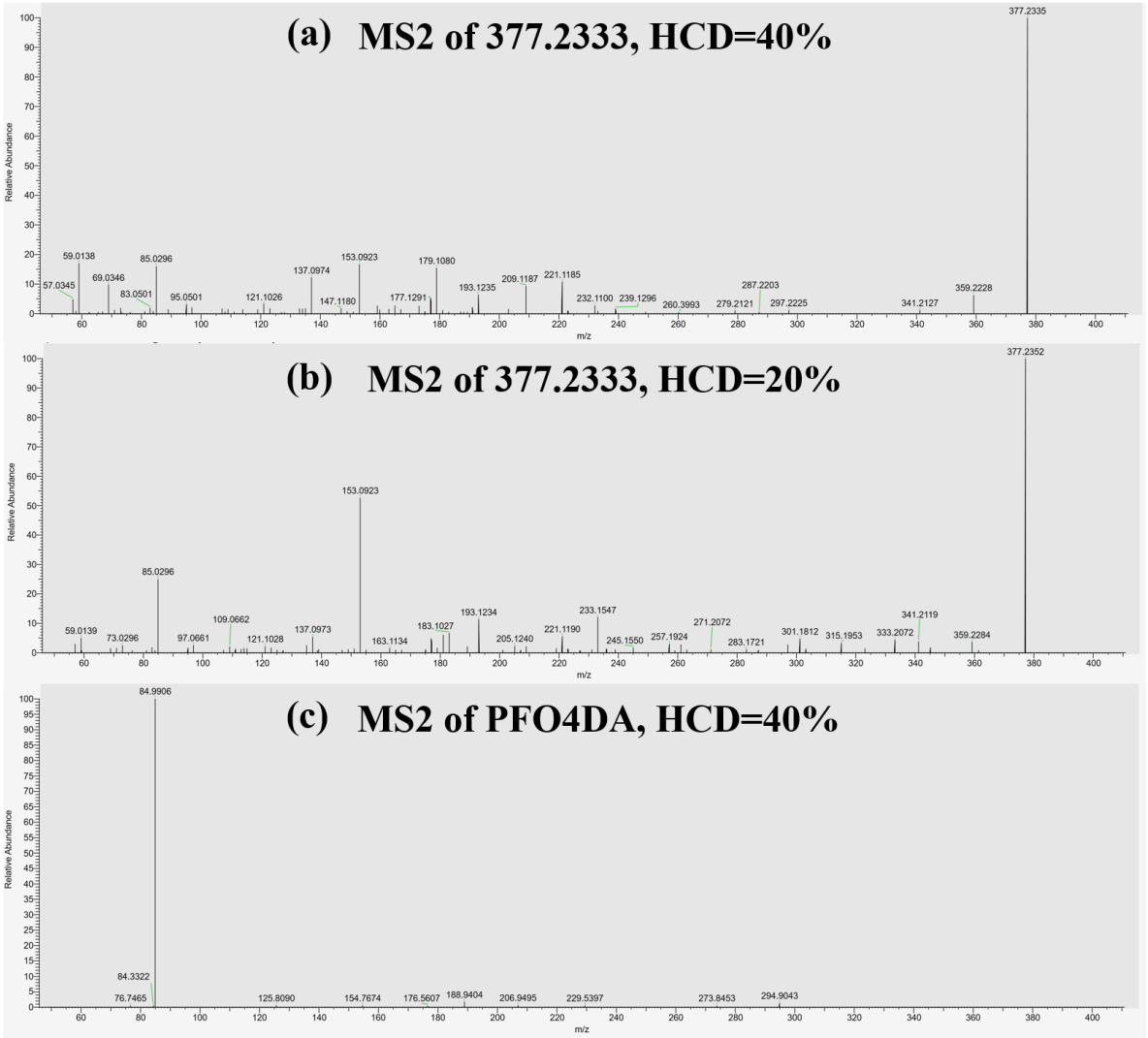


**Figure S3.** High resolution MS/MS spectrum of the interference peak and PFO4DA. Detailed LC and HRMS parameters can be found in Tables S2 and S3, respectively.

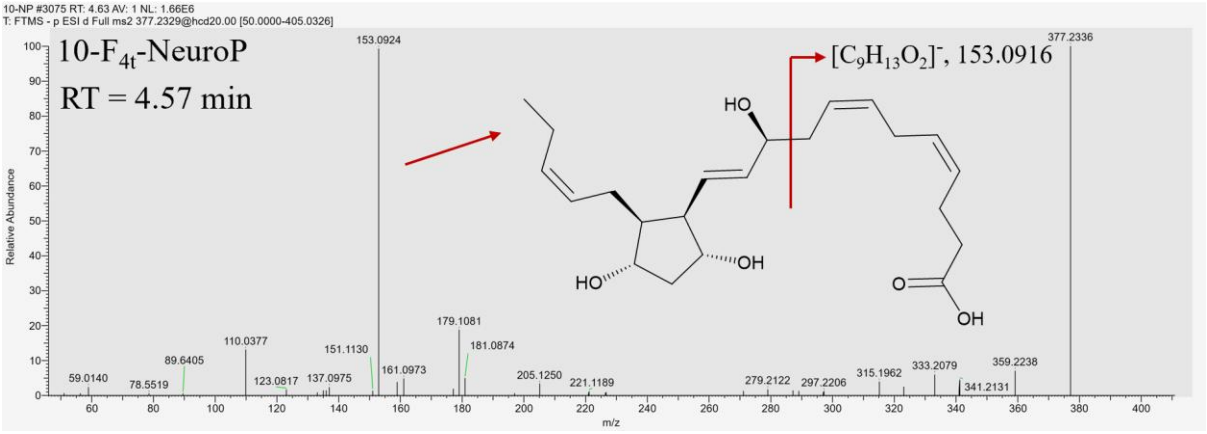


**Figure S4.** High resolution MS/MS spectrum of 10-$F_{4t}$-NeuroP in 1 µg/mL standard solution. Detailed LC and HRMS parameters can be found in Tables S2 and S3, respectively.

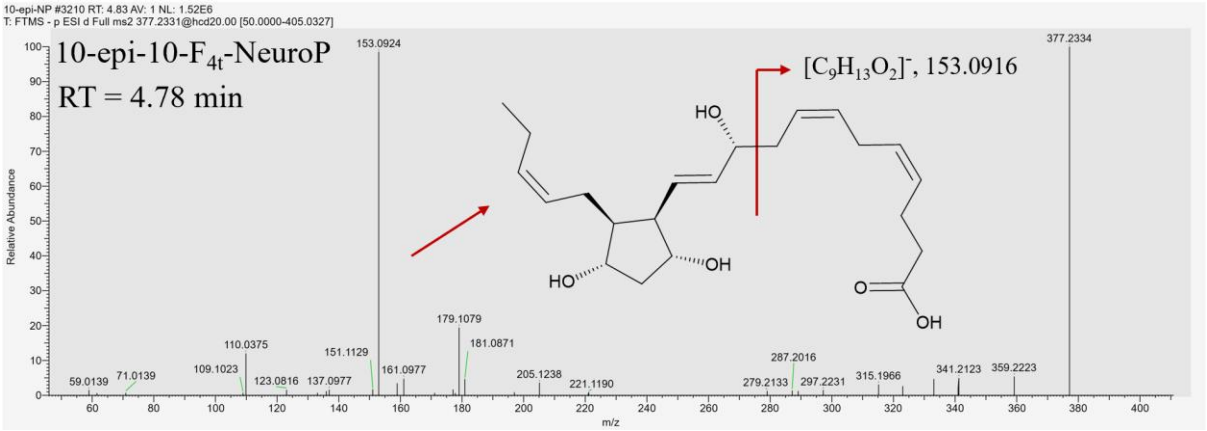


**Figure S5.** High resolution MS/MS spectrum of 10-epi-10-$F_{4t}$-NeuroP in 1 µg/mL standard solution. Detailed LC and HRMS parameters can be found in Tables S2 and S3, respectively.

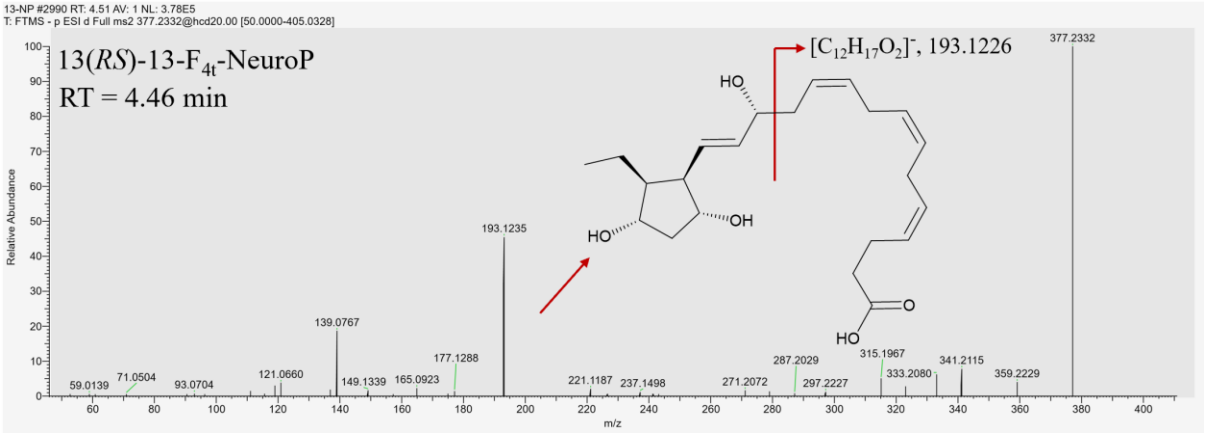


**Figure S6.** High resolution MS/MS spectrum of 13(*RS*)-13-$F_{4t}$-NeuroP in 1 µg/mL standard solution. Detailed LC and HRMS parameters can be found in Tables S2 and S3, respectively.

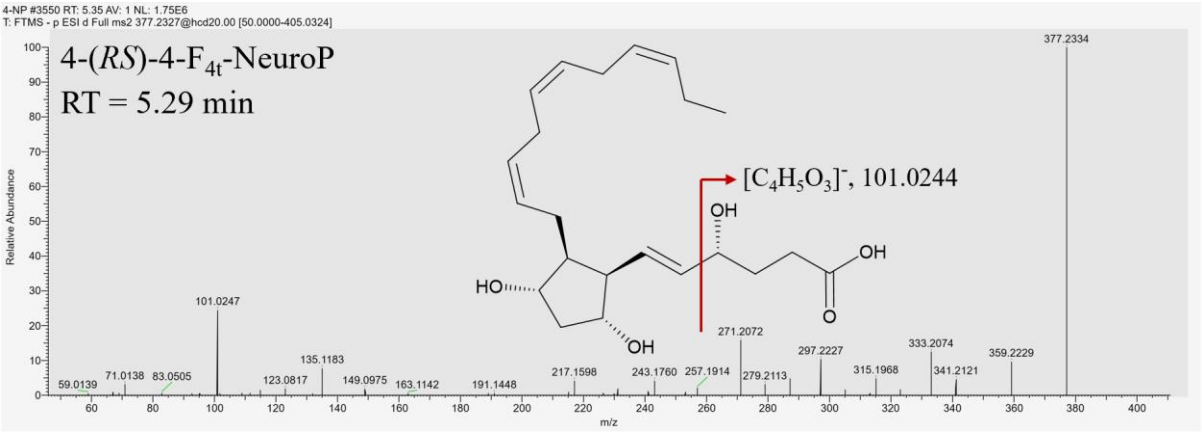


**Figure S7.** High resolution MS/MS spectrum of 4(*RS*)-$F_{4t}$-NeuroP in 1 µg/mL standard solution. Detailed LC and HRMS parameters can be found in Tables S2 and S3, respectively.

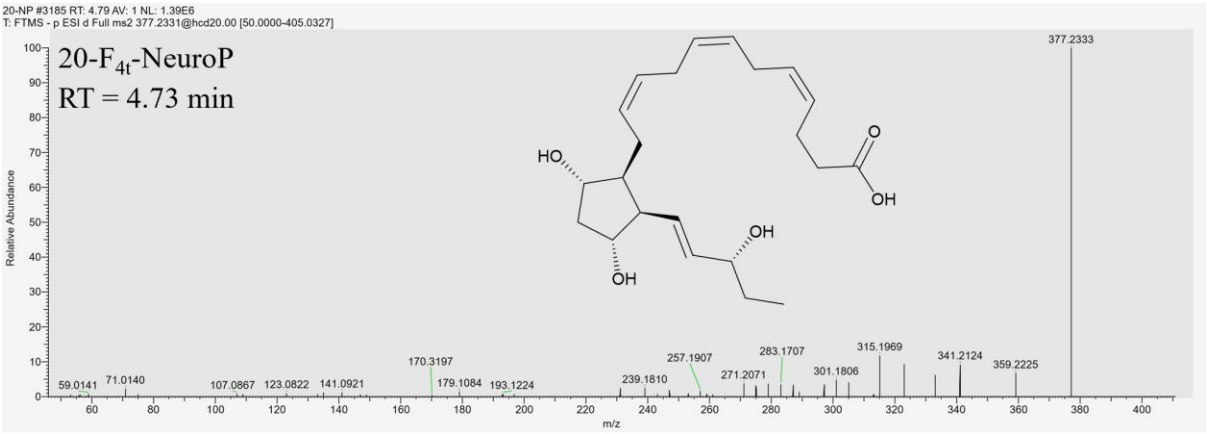


**Figure S8.** High resolution MS/MS spectrum of 20-$F_{4t}$-NeuroP in 1 µg/mL standard solution. Detailed LC and HRMS parameters can be found in Tables S2 and S3, respectively.

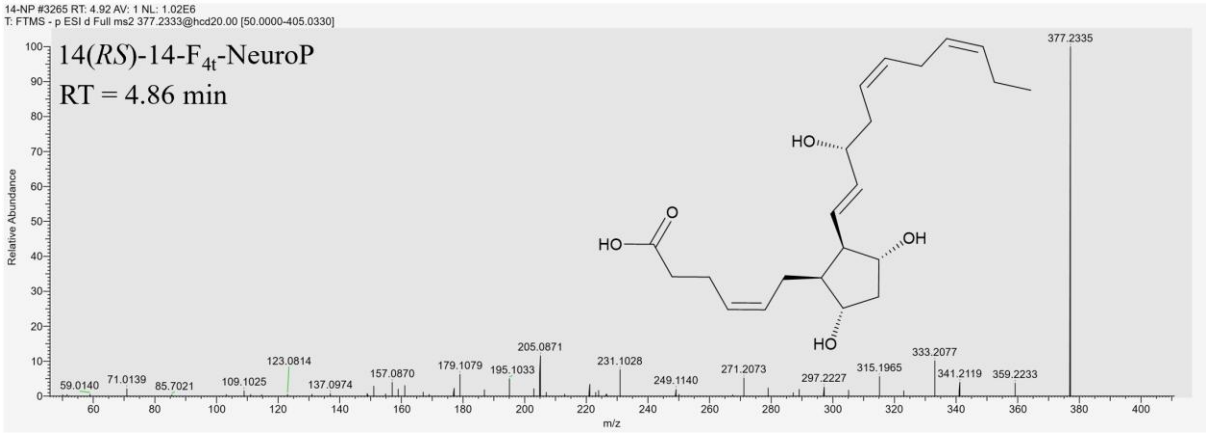


**Figure S9.** High resolution MS/MS spectrum of 14(*RS*)-14-$F_{4t}$-NeuroP in 1 µg/mL standard solution. Detailed LC and HRMS parameters can be found in Tables S2 and S3, respectively.

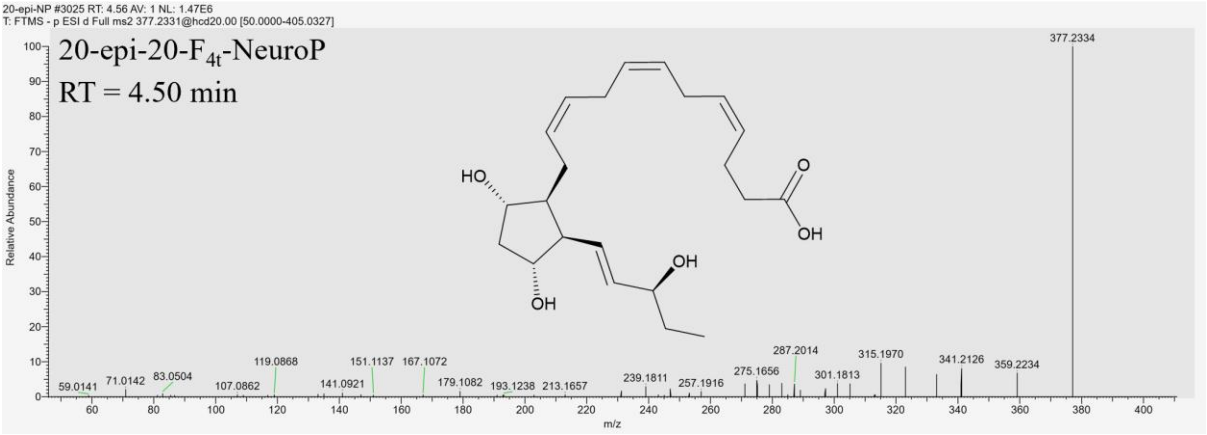


**Figure S10.** High resolution MS/MS spectrum of 20-epi-20-$F_{4t}$-NeuroP in 1 µg/mL standard solution. Detailed LC and HRMS parameters can be found in Tables S2 and S3, respectively.

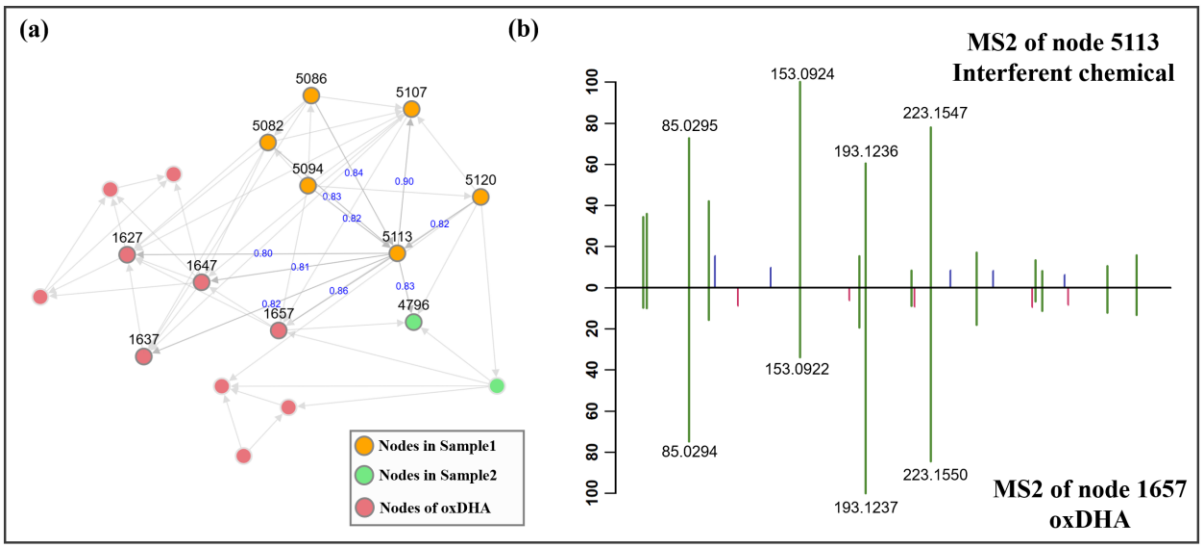


**Figure S11.** (a) Extract of the molecular network obtained with of the MS2 from the 377.2335 m/z of aquatic animal tested sample TS1 and TS2 and database of the in vitro oxidation of DHA (oxDHA). (b) MS2 spectrum comparation between interferent chemical in node 5113 and oxDHA in node 1657. The green line represents that the m/z of fragments from two nodes does not differ by more than 5 ppm.

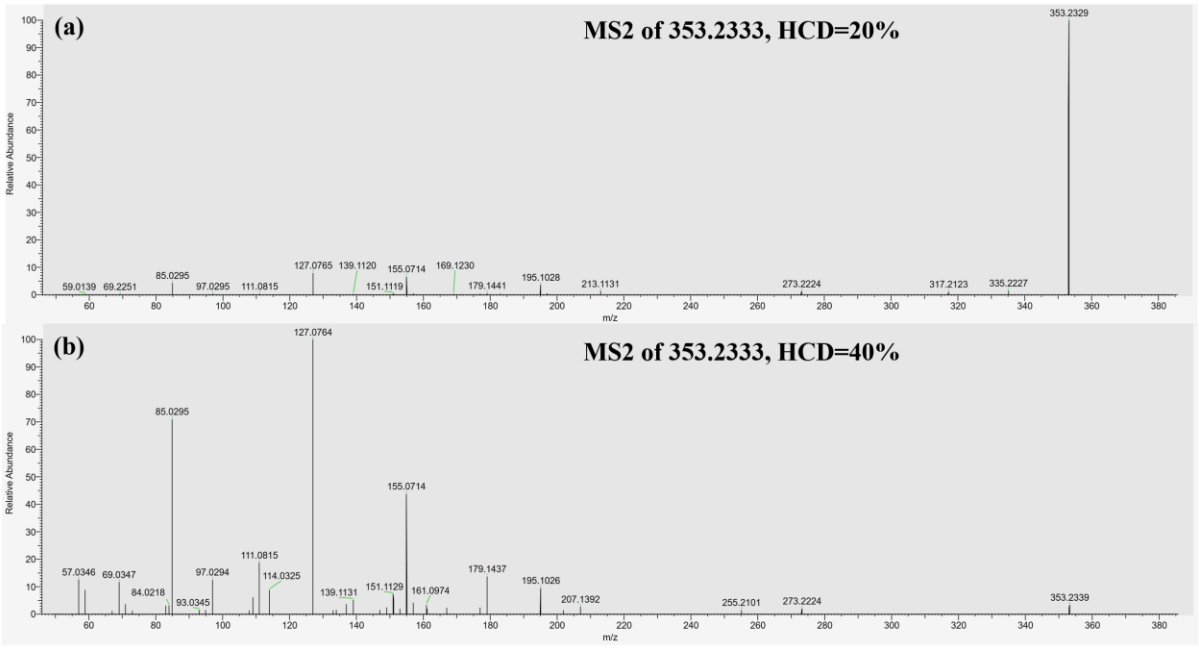


**Figure S12.** MS/MS spectra of Hepoxilin A3($HXA_3$) under high-resolution mass spectrometry. Detailed LC and HRMS parameters can be found in Tables S2 and S3, respectively.

**a)**

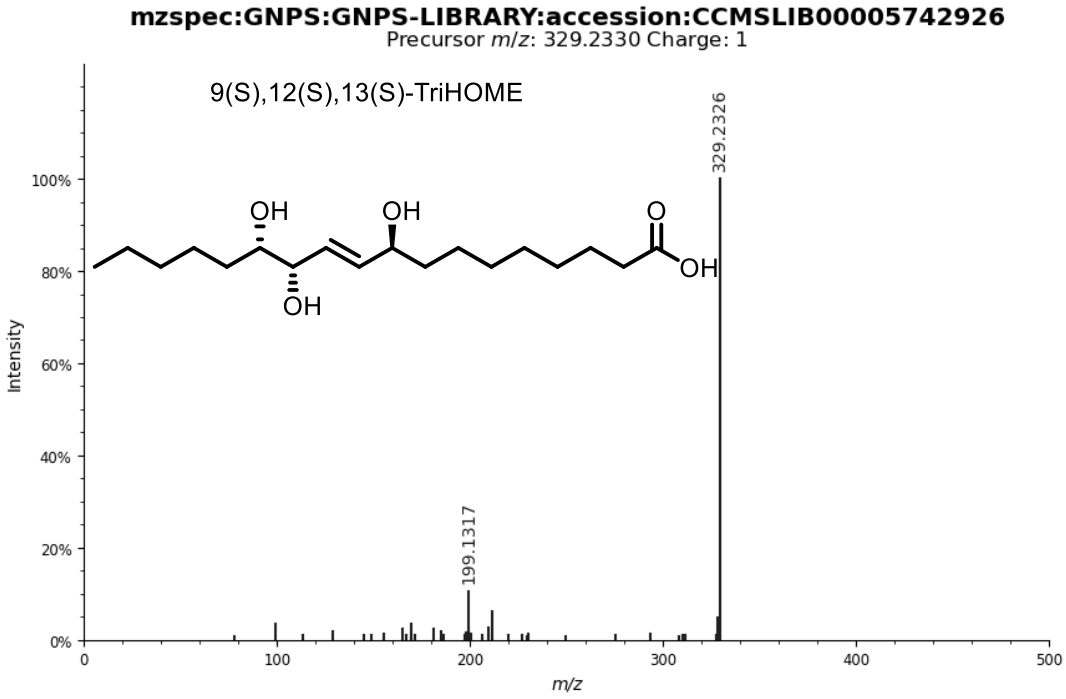


**b)**

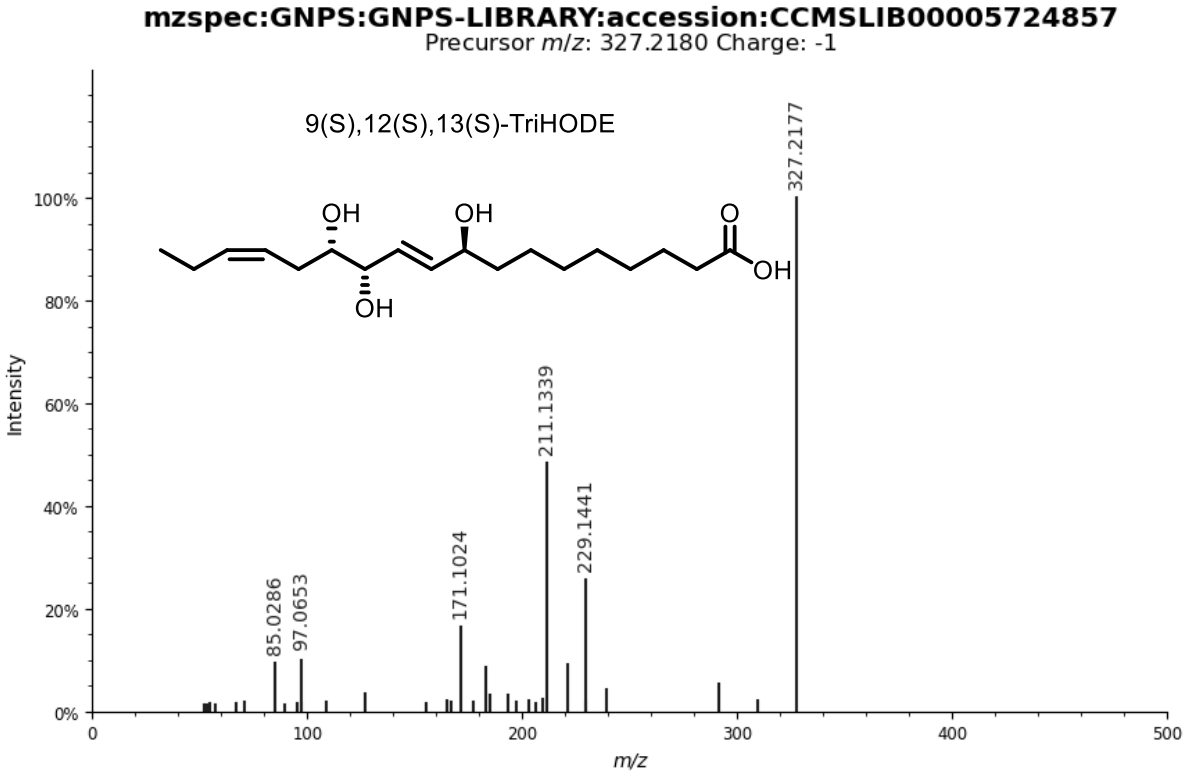


**Figure S13.** HRMS/MS Spectra retrieved from the GNPS library using smiles of a) 9,10,13-TriHOME ( CCCCC[C@H](O)[C@@H](O)/C=C/[C@@H](O)CCCCCCCC(O)=O ) and smiles of b) 9(S),12(S),13(S)-TriHODE (CC/C=C/CC(O)C(O)/C=C/C(O)CCCCCCCC(O)=O). Link to the original data is embedded in the picture.

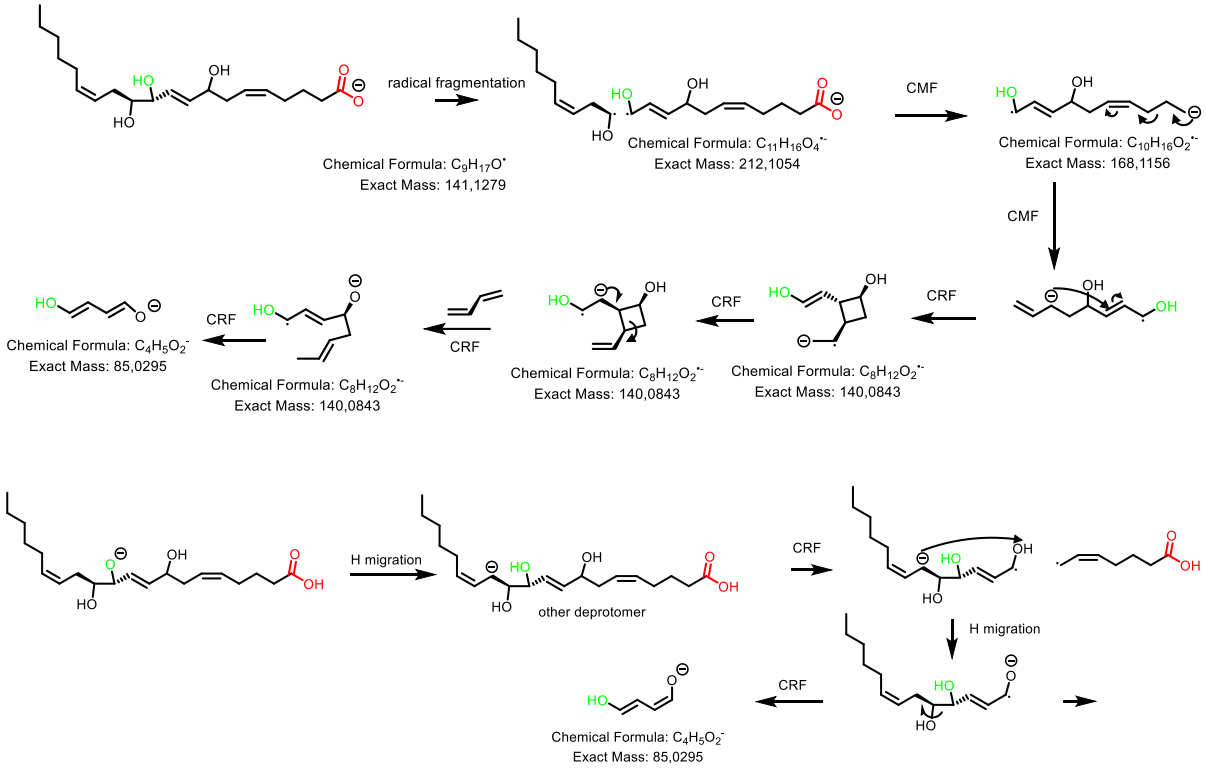


**Figure S14.** QCxMS Proposed fragmentation pathways to produce m/z 85.0295 from HXA3 deprotomer (deprotonation on the carboxylate and on the OH group)- CRF=charge retention fragmentation, CMF=charge migration fragmentation

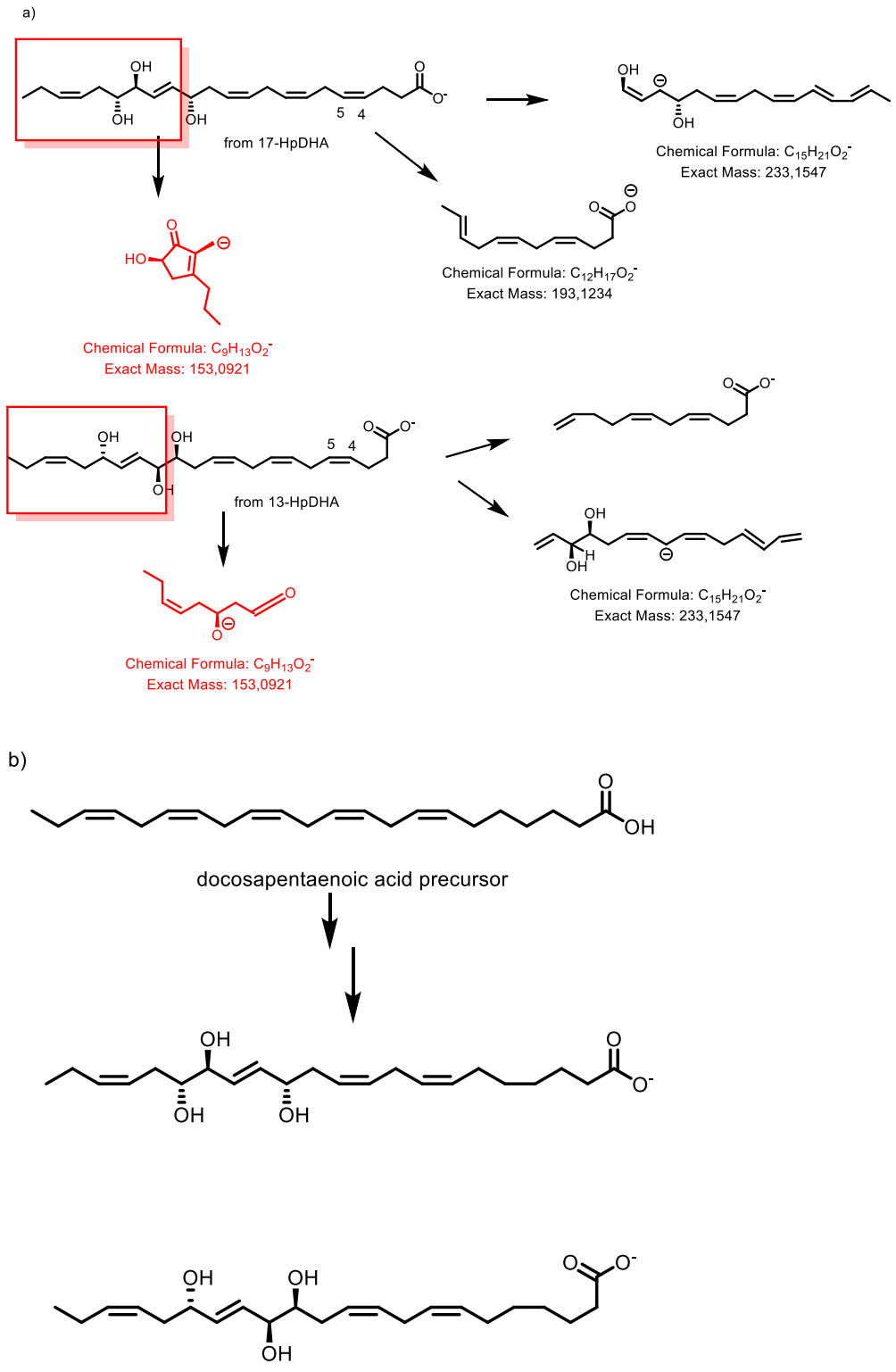


**Figure S15.** QcxMS proposed structures for the main fragments; those best match isomers from the simulation could not fit the + 2 Da addition depicted.

**a)**

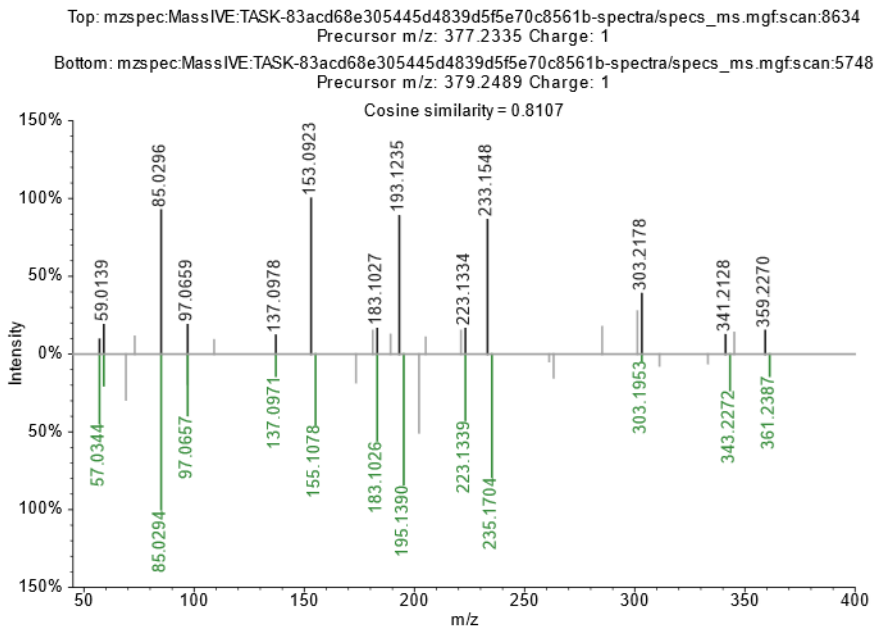


**b)**

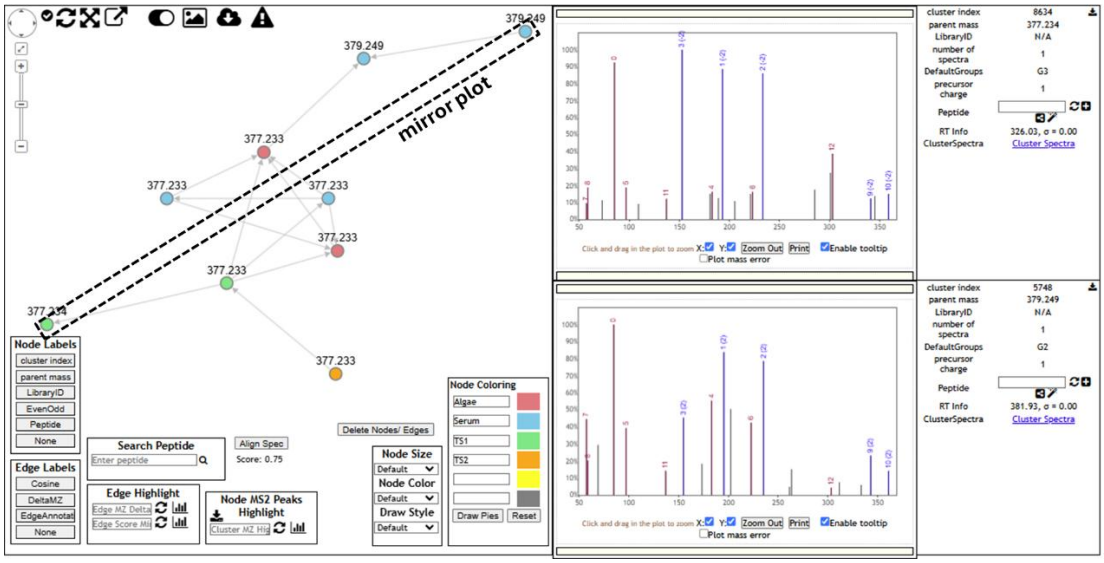


**Figure S16:** a) MS2 spectra mirror plot of the chemical interferent (m/z 377.233) and a oxylipin (m/z 379.249) suspecting to be of docosapentaenoic acid origin from the serum oxylipin extract '*Alignment_all_serum.mgf*' from Elloumi et al. dataset. It reveals similar chemical structures and the three main fragments to be shifted by +2.0156 Da (e.g., 153 to 155, 233 to 235, and 193 to 195). b) Extract of the molecular network obtained with the MS2 data from the aquatic animal tested sample TS1 and TS2 and from serum and algae oxylipins extracts from Elloumi et al. dataset. The network shows how the interferent is connected with their potential interferent isomers and those with a DPA oxylipin shown in a).

**Table S1.** The type of the samples, along with the sample numbers of each type.

| No. | Sample type | Sample number | Interference |
|---|---|---|---|
| 1 | Vegetables | 20 | No |
| 2 | Milk | 5 | No |
| 3 | Eggs | 5 | No |
| 4 | Pork | 5 | Yes |
| 5 | Mutton | 5 | Yes |
| 6 | Beef | 5 | Yes |
| 7 | Poultry | 5 | Yes |
| 8 | Fish | 15 | Yes |
| 9 | Shrimp | 5 | Yes |
| 10 | Cephalopod | 5 | Yes |
| 11 | Shellfish | 5 | Yes |
| 12 | Human breast milk | 20 | No |
| 13 | Human cord serum | 20 | Yes |
| 14 | River surface water | 2 | No |

Note: Human breast milk and cord serum samples were randomly selected from our existing inventory used in previous studies. Fish and river surface water was sampled in Shandong Province, China.

**Table S2.** Instrumental parameters for PFO4DA analysis by triple-quadrupole MS.

<table>
<tr><td>Instrument</td><td>ExionLC AD coupled to a QTRAP 6500 plus triple-quadrupole mass spectrometer (AB SCIEX, Framingham, MA, USA)</td></tr>
<tr><td>Column</td><td>Quantitation of PFO4DA:<br>Poroshell 120 EC-C18 (100 mm × 3 mm, 2.7 μm, Agilent, CA, USA)</td></tr>
<tr><td>Injection volume</td><td>5 μL</td></tr>
<tr><td>Mobile phase</td><td>A: 5 mM ammonium acetate in water, B: 5 mM ammonium acetate methanol</td></tr>
<tr><td>LC gradient</td><td>
<table>
<tr><th>Time (min)</th><th>Temp (℃)</th><th>Flow (mL/min)</th><th>A (%)</th><th>B (%)</th></tr>
<tr><td>0.0</td><td>40</td><td>0.4</td><td>60</td><td>40</td></tr>
<tr><td>3.5</td><td>40</td><td>0.4</td><td>10</td><td>90</td></tr>
<tr><td>7.0</td><td>40</td><td>0.4</td><td>10</td><td>90</td></tr>
<tr><td>7.1</td><td>40</td><td>0.4</td><td>60</td><td>40</td></tr>
<tr><td>9.0</td><td>40</td><td>0.4</td><td>60</td><td>40</td></tr>
</table>
</td></tr>
<tr><td>Mass parameters</td><td>Scan type: MRM<br>Scheduled MRM: Yes<br>Polarity: Negative<br>Source temperature: 200 ℃<br>Ion spray voltage: -3 000 V<br>Curtain gas: 30 psi<br>Collision gas: Medium<br>Ion source gas 1: 50 psi<br>Ion source gas 2: 55 psi</td></tr>
</table>

**Table S3.** MS parameters used in high-resolution spectrometry.

| | | |
|---|---|---|
| Instrument | | Exion LC coupled to an Orbitrap Exploris 120 (ThermoFisher, MA, USA) |
| Ion source type | | H-ESI |
| Spray voltage | | Static |
| Polarity | | Negative |
| Negative ion | | -1 000 V |
| Sheath gas | | 50 Arb |
| Aux gas | | 12.5 Arb |
| Sweep gas | | 0 Arb |
| Ion transfer tube temp | | 150 ℃ |
| Vaporizer temp | | 200 ℃ |
| MS1 | Resolution | 60 000 |
| | Scan range (m/z) | 80–1 000 |
| | RF Lens (%) | 50 |
| | Polarity | Negative |
| MS2 | Resolution | 15 000 |
| | Scan range (m/z) | 50–1 000 |
| | Collision energy mode | Fixed |
| | Acquisition mode | Data dependent acquisition |
| | HCD collision energy | 40% for PFAS; 20% for interference |
| | Inclusion list | m/z = 377.2333 and 376.9525 |
| | Isolation Window | 0.5 m/z |
| External mass calibration | | Pierce FlexMix |
| Internal calibration | | EASY-IC calibration |

**Table S4.** Names, retention times and main fragment in MS2 spectrum of the seven $F_{4t}$-NeuroP standards under UHPLC-high-resolution mass spectrometry.

| No. | Standard name | Retention time (min) | Main fragment | Fragment formular | MS2 spectrum |
|---|---|---|---|---|---|
| 1 | 10-$F_{4t}$-NeuroP | 4.57 | 153.0916 | $[C_9H_{13}O_2]^-$ | Figure S4 |
| 2 | 10-epi-10-$F_{4t}$-NeuroP | 4.78 | 153.0916 | $[C_9H_{13}O_2]^-$ | Figure S5 |
| 3 | 13(*RS*)-13-$F_{4t}$-NeuroP | 4.46 | 193.1221 | $[C_{12}H_{17}O_2]^-$ | Figure S6 |
| 4 | 4(*RS*)-$F_{4t}$-NeuroP | 5.29 | 101.0244 | $[C_4H_5O_3]^-$ | Figure S7 |
| 5 | 20-$F_{4t}$-NeuroP | 4.73 | / | / | Figure S8 |
| 6 | 14(*RS*)-14-$F_{4t}$-NeuroP | 4.86 | / | / | Figure S9 |
| 7 | 20-epi-20-$F_{4t}$-NeuroP | 4.50 | / | / | Figure S10 |

**Table S5.** MZmine3 and GNPS parameters.

| **MZmine3 parameters** | | |
|---|---|---|
| MS detection | MS1 intensity threshold | 5.0E05 |
| | MS2 intensity threshold | 1.0E04 |
| | Minimum consecutive scans | 5 |
| | Tolerance | 5 ppm |
| Deconvolution | Chromatographic threshold | 30% |
| | Minimum search range RT | 0.04 |
| | Minimum relative height | 2% |
| | Min ratio of peak top/edge | 1 |
| | Peak duration range | 0.05-0.50 min |
| | Minimum scans | 5 |
| MSMS merged | m/z merge mode | weighted average |
| | Intensity merge mode | sum intensities |
| | Expected mass deviation | 5 ppm |
| | Cosine threshold | 70.0% |
| | Signal count threshold | 20.0% |
| | Isolation window width | 0.5 m/z |
| **GNPS matching parameters** | | |
| Minimum cosine score | | 0.6 |
| Minimum matching peaks | | 5 |
| Precursor error | | 5 mDa |
| Product ion error | | 5 mDa |
| MSMS filtering options | | default |

**Table S6.** Concentrations (in ng/g) of PFAS in river water and fish samples.

| Sample | PFMOAA | PFO2HxA | PFO3OA | PFO4DA | PFO4DA (Interfered) | PFO5DoA | PFOA | PFOS |
|---|---|---|---|---|---|---|---|---|
| River 1 | 0.912 | 0.875 | 0.486 | 0.019 | / | 0.004 | 1.501 | 0.005 |
| River 2 | 2.657 | 2.012 | 1.317 | 0.108 | / | 0.013 | 17.198 | 0.014 |
| Fish 1 | 5.963 | 0.590 | 0.726 | 0.156 | 2.342 | 0.468 | 56.910 | 24.512 |
| Fish 2 | 6.835 | 0.426 | 0.741 | 0.091 | 5.618 | 0.585 | 44.686 | 55.357 |
| Fish 3 | 13.298 | 1.667 | 1.041 | 0.160 | 4.865 | 1.033 | 95.295 | 71.127 |
| Fish 4 | 19.436 | 1.518 | 1.355 | 0.197 | 7.562 | 0.808 | 71.889 | 63.447 |
| Fish 5 | 27.420 | 1.827 | 4.165 | 0.193 | 6.344 | 1.083 | 121.434 | 69.547 |
| Fish 6 | 147.776 | 17.216 | 7.137 | 1.071 | 13.599 | 5.557 | 565.294 | 82.148 |
| Fish 7 | 80.724 | 11.252 | 6.124 | 0.968 | 15.195 | 3.003 | 304.575 | 66.269 |
| Fish 8 | 94.552 | 16.840 | 7.466 | 0.986 | 15.413 | 3.806 | 324.958 | 70.385 |
| Fish 9 | 209.957 | 10.539 | 4.355 | 1.039 | 15.901 | 6.180 | 404.571 | 76.575 |
| Fish 10 | 84.098 | 6.579 | 3.266 | 0.947 | 13.981 | 2.201 | 241.356 | 58.681 |

**Note:** Fish samples 1-5 were sampled from River 1 site and Fish samples 6-10 were from River 2 site.